

Charge Transfer Excitations in Insulating Copper Oxides

A.S. Moskvina,¹ S.-L. Drechsler,² R. Hayn,^{2,3} and J. Málek^{2,4}

¹Ural State University, 620083 Ekaterinburg, Russia

²Leibniz-Institut für Festkörper- und Werkstoffforschung Dresden, P.O. Box 270116, D-01171 Dresden, Germany

³Laboratoire Matériaux et Microélectronique de Provence,

Université Paul Cézanne, Case 142, F-13397 Marseille Cedex 20, France

⁴Institute of Physics, ASCR, Na Slovance 2, CZ-18221 Praha 8, Czech Republic

(Dated: August 26, 2016)

A semi-quantitative cluster approach is developed to describe the charge transfer (CT) electron-hole excitations in insulating cuprates in a rather wide energy range up to $10 \div 15$ eV. It generalizes the Zhang-Ng (ZN) model of CT excitons by considering the complete set of Cu $3d$ and O $2p$ orbitals within the CuO_4 embedded molecular cluster method and by introducing one-center (intra-center) Frenkel-like and two-center (inter-center) excitons. Special attention is paid to the transition matrix element effects both in optical and electron energy loss spectra (EELS). In the latter case we obtain the momentum dependence of matrix elements both for intra-center and inter-center transitions. We are able to give a semi-quantitative description of the optical and EELS spectra for a large number of 0D (like CuB_2O_4), 1D (Sr_2CuO_3) and 2D (like $\text{Sr}_2\text{CuO}_2\text{Cl}_2$) insulating cuprates in a unifying manner. By comparing our analysis with the experimental data we find that the CT gap in insulating cuprates is determined by nearly degenerate intra-center localized excitations and inter-center CT excitons. The former are associated with a hole CT transition $b_{1g} \rightarrow e_u(\pi)$ from the $b_{1g} \propto d_{x^2-y^2}$ ground state of dominantly Cu $3d_{x^2-y^2}$ character to a purely oxygen dominantly O $2p_\pi$ state localized on one CuO_4 plaquette, whereas the latter correspond to a $b_{1g} \rightarrow b_{1g}$ CT transition between neighboring plaquettes with the Zhang-Rice (ZR) singlet being the final two-hole state. The corresponding EELS intensity is found to be strongly \mathbf{k} dependent: even for isolated exciton it sharply decreases by approaching the Brillouin zone (BZ) boundary. It is shown that the interaction of two-center excitons can result in destructive interference effects with an intensity compensation point.

I. INTRODUCTION

The nature of the electron-hole excitations in parent quasi-2D cuprates such as La_2CuO_4 , $\text{Sr}_2\text{CuO}_2\text{Cl}_2$, $\text{YBa}_2\text{Cu}_3\text{O}_6$, and their 1D counterparts like Sr_2CuO_3 , Sr_2CuO_2 , Li_2CuO_2 represents an important challenging issue both for the high- T_c problem and, more generally, for strongly correlated oxides. The mechanism of low-energy electron-hole excitations as well as those with higher energy and high intensity is still unclear.

It is now widely believed that the most intensive low-energy electronic excitations in quasi-2D insulating copper oxides correspond to the transfer of electrons from O to Cu in the CuO_2 layer, hence these materials are charge transfer (CT) insulators.¹ Moreover, sometimes the intensive band near $2 \div 3$ eV is naively supposed to be the only representative of the O $2p$ -Cu $3d$ charge transfer, and higher-lying structures are assigned to transitions relevant to Cu $4s$, La $5d/4f$, Sr $5d$, or Ca $4d$ depending on the actual chemical formula of the corresponding cuprate.

Despite the giant ($\sim 10^4$) number of experimental and theoretical papers on cuprates we deal actually with a lack of detailed studies of electron-hole excitations both in parent and high- T_c cuprates. The most part of optical information² was obtained to date by reflectivity measurements followed by a Kramers-Kronig transformation usually accompanied by a number of unavoidable uncertainties as regards the peak positions

and intensities of weak spectral features. Nevertheless, applying different optical measurements including Raman spectroscopy and nonlinear susceptibility, one obtains important information, in particular, as regards the subtleties of the optical gap states in such insulating cuprates as CuO ,^{3,4} La_2CuO_4 ,^{5,6,7,8} R_2CuO_4 ($\text{R}=\text{La}$, Nd , Eu , Gd),^{7,9} $\text{YBa}_2\text{Cu}_3\text{O}_6$,^{10,11} $\text{Sr}_2\text{CuO}_2\text{Cl}_2$,^{12,13,14,15} and Sr_2CuO_3 .^{16,17,18}

Unfortunately, any conventional optical technique is momentum restricted, and yields an *indirect* information on the dielectric function $\epsilon(\omega, \mathbf{k})$ only at the Γ -point given by $\mathbf{k} \rightarrow 0$. In other words, such a technique cannot probe the dynamics of electron-hole excitations.

In this connection, we would like to emphasize the decisive role of *direct* EELS measurements in the observation and analysis of electron-hole excitations as compared with conventional *indirect* optical data. The possibility to yield the polarization and momentum dependent loss function $\text{Im}(-1/\epsilon(\omega, \mathbf{k}))$ makes EELS a powerful tool to examine subtle details of the energy spectrum and dynamics of electron-hole excitations in cuprates.^{19,20,21} In the limit $\mathbf{k} \rightarrow 0$ the selection rules are the same as in optics, i.e. only dipole transitions are allowed. For finite \mathbf{k} nondipole transitions are detected as well. In contrast to reflectivity measurements, the EELS in transmission is a surface insensitive technique. Recently, momentum resolved resonant inelastic X-ray scattering (RIXS) measurements^{22,23} performed for $\text{Sr}_2\text{CuO}_2\text{Cl}_2$ and $\text{Ca}_2\text{CuO}_2\text{Cl}_2$ have demonstrated the feasibility of RIXS to study electron-hole excitations in

insulating cuprates.

The theoretical analysis of optical excitations beyond simple band models has been mostly performed in the frame of conventional Hubbard-like models, where one usually considers only O $2p_\sigma$ orbitals, and neglects O $2p_\pi$ and O $2p_z$ orbitals at all. In the parameter regime appropriate for undoped cuprates, one implies that the one hole per unit cell is mainly localized on the Cu site. Application of the current operator onto this state provides a charge transfer from the Cu to the O site. Thus, one would expect a dominant absorption feature at the energy of the charge transfer gap. In terms of the Hubbard model, this is a CT transition from the nonbonding oxygen to the upper Hubbard band. It was emphasized that instead of a transition to the upper Hubbard band, it is more reasonable to speak of a transition to the correlated Zhang-Rice²⁴ type states.²⁵

One of the central issues in the analysis of electron-hole excitations is whether low-lying states are comprised of free charge carriers or excitons. A conventional approach implies that if the Coulomb interaction is effectively screened and weak, then the electrons and holes are only weakly bound and move essentially independently as free charge-carriers. However, if the Coulomb interaction between electron and hole is strong, excitons are formed, i.e. bound particle-hole pairs with strong correlation of their mutual motion. In practice, many authors consider excitons to consist of real-space configurations with electrons and holes occupying nearest neighbor sites, while the electrons and holes are separated from each other in the conduction-band states.²⁶

The electron-hole excitations near the CT gap in insulating CuO_2 planes were theoretically examined in Ref. 27 in terms of a six-band model and using the cell-perturbation method. The excitons were approximately treated as electrons and holes moving freely in their respective quasi-particle bands, except in the nearest neighborhood, where they feel an attraction and an on-site interaction determined by the eigenstate of the cell Hamiltonian, which leads to a rather small exciton dispersion.

However, a small exciton dispersion is in contradiction to the results of the EELS measurements for the 2D model cuprate $\text{Sr}_2\text{CuO}_2\text{Cl}_2$.¹⁹ These measurements stimulated the elaboration of a simple CT exciton model by Zhang and Ng.^{19,28} They used a local model to study the formation and the structure of the low-energy charge-transfer excitations in the insulating CuO_2 plane restricting themselves to the Cu $3d_{x^2-y^2}$ and O $2p_\sigma$ orbitals. The elementary excitation is a bound exciton of spin singlet, consisting of a Cu^+ and a neighboring Zhang-Rice singlet-like excitation of Cu-O holes with a rather large dispersion. They considered four eigenmodes of excitons with different symmetry A_{1g} , B_{1g} , E_u , or S , D , $P_{1,2}$. The experimental peak analysis in $\text{Sr}_2\text{CuO}_2\text{Cl}_2$ revealed a surprisingly large energy dispersion ≈ 1.5 eV along $[110]$ which was interpreted in terms of a small exciton moving through the lattice freely without disturbing the antiferromagnetic spin background, in contrast to the single

hole motion.^{19,28} So, it seems that the situation in antiferromagnetic cuprates differs substantially from that in usual semiconductors or in other bandlike insulators where, as a rule, the effective mass of the electron-hole pair is larger than that of an unbound electron and hole.

Other theoretical works in the frame of conventional Hubbard-like models, without the O $2p_\pi$ and $2p_z$ orbitals, are those by Hanamura *et. al.*²⁹ and Kuzian *et. al.*³⁰ The *excitonic cluster model*²⁹ has been elaborated to describe the CT transitions in insulating cuprates in frame of the conventional three-band Hubbard Hamiltonian. The authors made an attempt to treat both the bound and unbound states of the CT electron-hole pair on the same footing. To this end they performed perturbation calculation for the excited states of E_u symmetry generated by the oxygen O $2p_\sigma$ hole separated from the Cu $3d_{x^2-y^2}$ electron by distances of 1, 2, 3, 4, or 5 nearest neighbors. To evaluate the dipole transition matrix element they took into account only the transition between the $d_{x^2-y^2}$ and the O $2p_\sigma$ orbital of e_u symmetry. The frequency and wave number dependence of the dielectric function $\epsilon(\mathbf{k}, \omega)$ and its inverse $\epsilon^{-1}(\mathbf{k}, \omega)$ has also been studied in Ref. 30. The authors show that the problem, in general, cannot be reduced to a calculation within the single band Hubbard model, which takes into account only a restricted number of electronic states near the Fermi energy. The contribution of the rest of the system to the longitudinal response is essential for the whole frequency range. With the use of the spectral representation of the two-particle Green's function they show that the problem may be divided into two parts: into the contributions of the weakly correlated and the Hubbard subsystems. For the latter an approach is proposed that starts from the correlated paramagnetic ground state with strong antiferromagnetic fluctuations. The method is applied to the multiband Hubbard (Emery) model that describes layered cuprates.

Already a shorthand inspection of the original experimental data,¹⁹ and especially of the high-resolution EELS spectra^{20,21} for $\text{Sr}_2\text{CuO}_2\text{Cl}_2$ point to some essential shortcomings of the Zhang-Ng (ZN) model. The high-resolution EELS spectra^{20,21} for insulating $\text{Sr}_2\text{CuO}_2\text{Cl}_2$ with a momentum range along $[110]$ broader than in Ref. 19 did not confirm two principal predictions of the ZN-model: no spots of the predicted D -mode exciton were found in a broad energy range below 2 eV; a clear decrease contrary to the predicted increase of EELS intensity along $[100]$ was observed with momentum increase from $k = 0.5$ to $k = 0.7$. Moreover, the high-resolution measurements^{20,21} unambiguously detected a "multi-excitonic" nature of EELS spectra in the $2 \div 8$ eV energy range with a clear manifestation of several dispersionless narrow bands with energies near 2.0, 4.2, 5.4, and 7.2 eV. Thus, we conclude that the simple ZN model should be revisited to consistently explain the large body of new experimental data.

Especially important is the proper inclusion of the O $2p_\pi$ orbitals into the theory of electron-hole excitations.

One of the first microscopic models for the low-energy CT transition in the insulating copper oxide CuO peaked near 1.7 eV was given in Ref. 3. This transition was assigned to the dipole-allowed CT transition $b_{1g} \rightarrow e_u$ from the Cu $3d$ -O $2p$ hybrid $b_{1g} \propto d_{x^2-y^2}$ hole ground state to the purely oxygen orbital doublet e_u state with predominant O $2p_\pi$ weight. To the best of our knowledge, it was the first indication of an optical manifestation of low-lying nonbonding O $2p_\pi$ states.

In the present work we generalize the ZN-theory into a simple, physically clear, cluster theory for the CT excitons that on the one hand catches the essential physics and on the other hand provides a semi-quantitative description of the optical and EELS spectra. A preliminary analysis^{31,32} has shown that a concise interpretation of the experimental EELS spectra may be obtained by developing further the ZN-model with respect to two points. First of all, we include the complete set of Cu $3d$ and O $2p$ orbitals of the plaquette in terms of the embedded cluster method. And second, we argue that the elementary O-Cu CT process^{19,28} generates two types of excitons: one-center excitons localized on one CuO₄ plaquette and two-center excitons extending over two CuO₄ plaquettes. We base our argumentation mainly on the \mathbf{k} dependence of the corresponding EELS intensity as revealed by a detailed analysis of matrix elements of one- and two-center excitons. We also investigate the exciton dynamics. Finally we arrive at a semi-quantitative understanding of the electronic states that dominate the optical and EELS response in a rather broad energy range. In such a way we explain the main features of optical and angle-resolved EELS spectra for a large number of different cuprates. They reach from the 0D compound CuB₂O₄, over the 1D cuprate Sr₂CuO₄ up to the 2D model compound Sr₂CuO₂Cl₂ and the parent cuprates of high- T_c superconductors. For instance, we present an alternative explanation of the angle-resolved EELS spectra of Sr₂CuO₂Cl₂ that is free from many shortcomings of the ZN-model. We should emphasize that our theory, like also those of Zhang and Ng cannot provide a proof whether the low-lying particle-hole pairs are bound or not. It has to be expected that at least the higher lying particle-hole excitations on a finite cluster do in reality not exist as quasi-particle excitations with infinite life time. Nevertheless, they should be visible in the spectra as resonances, having possibly a rather large broadening. In that sense, we will denote *all* particle-hole excitations as *excitons* in the present paper. The question of its life time has to be answered independently. Therefore, we cannot contribute for example to the ongoing discussion about the stability of long-lived excitons in 1D cuprates.^{33,34,35}

The rest of the paper is organized as follows. In Sec. II we shortly address the electronic structure and the energy spectrum of a CuO₄ cluster. The one-center small excitons with appropriate transition matrix elements are considered in Sec. III. The two-center small excitons and accompanying issues of correlations, final state effects,

EELS transition matrix elements, even and odd excitons are addressed in Sec. IV. In Sec. V we address the problem of the energy and intensity dispersion of two-center excitons. Sec. VI is devoted to a model analysis of the experimental EELS spectra in 0D, 1D and 2D insulating cuprates.

II. ELECTRONIC STRUCTURE OF COPPER-OXYGEN CLUSTERS

The electronic states in strongly correlated cuprates manifest both significant correlations and dispersive features. The dilemma posed by such a combination is the overwhelming number of configurations which must be considered in treating strong correlations in a truly bulk system. One strategy to deal with this dilemma is to restrict oneself to small clusters, creating model Hamiltonians whose spectra may reasonably well represent the energy and dispersion of the important excitations of the full problem. Naturally, such an approach has a number of principal shortcomings, including the boundary conditions, the breaking of local symmetry of boundary atoms, and so on.

As an efficient approach to describe excitonic states, especially with small effective electron-hole separation we propose here the embedded molecular cluster method. In the present context we use one or two neighboring CuO₄ clusters embedded into the insulating cuprate. This method provides both, a clear physical picture of the complex electronic structure and the energy spectrum, as well as the possibility of quantitative modelling. Eskes *et al.*³⁶, as well as Ghijsen *et al.*³⁷ have shown that in a certain sense the cluster calculations might provide a better description of the overall electronic structure of insulating copper oxides than band-structure calculations. They allow to take better into account correlation effects.

Beginning from 5 Cu $3d$ and 12 O $2p$ atomic orbitals for CuO₄ cluster with D_{4h} symmetry, it is easy to form 17 symmetrized $a_{1g}, a_{2g}, b_{1g}, b_{2g}, e_g$ (gerade=even) and $a_{2u}, b_{2u}, e_u(\sigma), e_u(\pi)$ (ungerade=odd) orbitals. The even Cu $3d$ $a_{1g}(3d_{z^2}), b_{1g}(3d_{x^2-y^2}), b_{2g}(3d_{xy}), e_g(3d_{xz}, 3d_{yz})$ orbitals hybridize, due to strong Cu $3d$ -O $2p$ covalency, with even O $2p$ -orbitals of the same symmetry, thus forming appropriate bonding γ^b and antibonding γ^a states. Among the odd orbitals only $e_u(\sigma)$ and $e_u(\pi)$ hybridize due to nearest neighbor pp overlap and transfer thus forming appropriate bonding e_u^b and antibonding e_u^a purely oxygen states. The purely oxygen a_{2g}, a_{2u}, b_{2u} orbitals are nonbonding. All "planar" O $2p$ orbitals (see Fig. 1) in accordance with the orientation of lobes could be classified as σ ($a_{1g}, b_{1g}, e_u(\sigma)$) or π ($a_{2g}, b_{2g}, e_u(\pi)$) orbitals, respectively.

Bonding and antibonding molecular orbitals in hole representation can be presented as

$$|\gamma^b\rangle = \cos \alpha_\gamma |\gamma(3d)\rangle + \sin \alpha_\gamma |\gamma(2p)\rangle,$$

$$|\gamma^a\rangle = \sin \alpha_\gamma |\gamma(3d)\rangle - \cos \alpha_\gamma |\gamma(2p)\rangle.$$

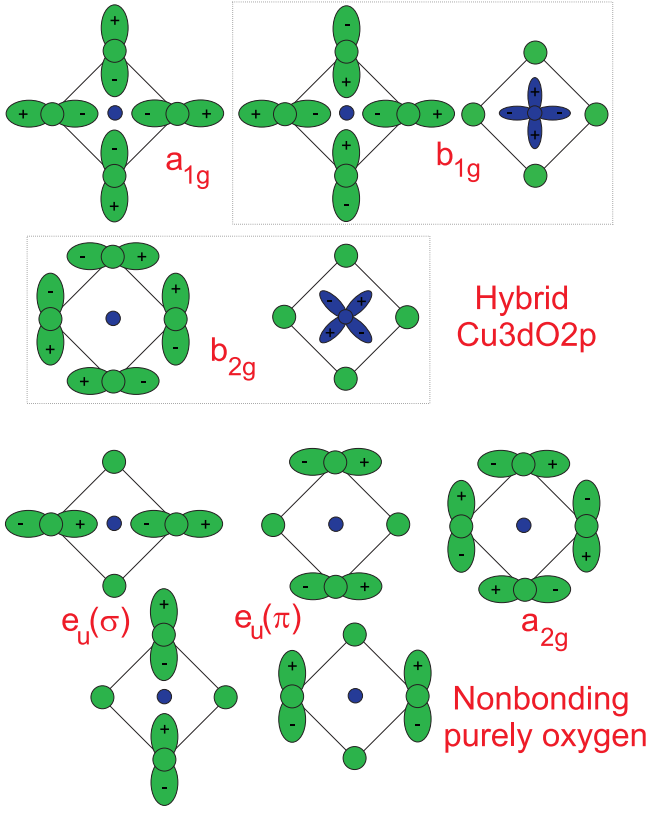


FIG. 1: Electron (hole) density distribution for planar copper and oxygen molecular orbitals of one CuO_4 plaquette.

For example,

$$|b_{1g}^b\rangle = \cos \alpha_{b_{1g}} |b_{1g}(3d)\rangle + \sin \alpha_{b_{1g}} |b_{1g}(2p)\rangle,$$

$$|b_{1g}^a\rangle = \sin \alpha_{b_{1g}} |b_{1g}(3d)\rangle - \cos \alpha_{b_{1g}} |b_{1g}(2p)\rangle, \quad (1)$$

where $b_{1g}(3d) = 3d_{x^2-y^2}$;

$$|e_u^b\rangle = \cos \alpha_e |e_u(\pi)\rangle + \sin \alpha_e |e_u(\sigma)\rangle,$$

$$|e_u^a\rangle = \sin \alpha_e |e_u(\pi)\rangle - \cos \alpha_e |e_u(\sigma)\rangle \quad (2)$$

equally for both types (x, y) of such orbitals.

To explain the electronic structure of the embedded molecular cluster in a broad energy range we need the complete information about the bare parameters of the effective Hamiltonian. The numerical values of energy parameters for holes in insulating cuprates like La_2CuO_4 or $\text{Sr}_2\text{CuO}_2\text{Cl}_2$ which were used by different authors^{38,39,40,41,42} can be summarized as follows (in eV):

$$\epsilon_p - \epsilon_d \approx 2$$

$$\epsilon_{p\sigma} - \epsilon_{p\pi} \approx 1 \div 3; \quad \epsilon_{p\pi} < \epsilon_{pz} < \epsilon_{p\sigma};$$

$$U_d \approx 6 \div 10 \text{ eV}; \quad U_p \approx 4 \div 6; \quad V_{pd} \approx 0.5 \div 1.5;$$

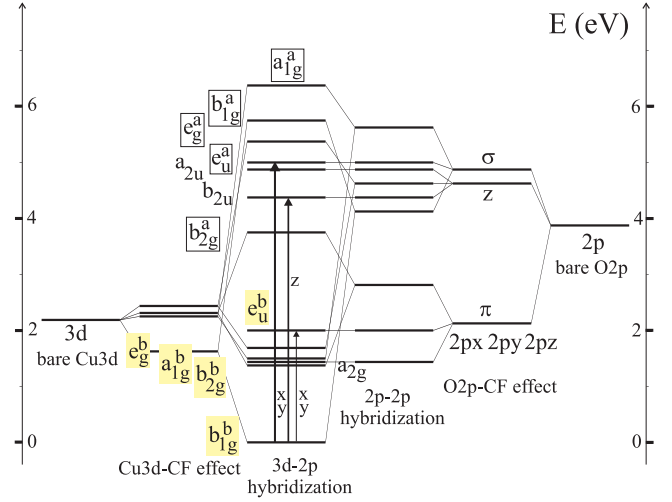


FIG. 2: Model single-hole energy spectra for a CuO_4 plaquette with parameters relevant for $\text{Sr}_2\text{CuO}_2\text{Cl}_2$ and a number of other insulating cuprates.

$$t_{pd} \approx 1.0 \div 1.5; \quad |t_{pp\sigma}| \approx 0.8; \quad t_{pp\pi} \approx \frac{1}{2}|t_{pp\sigma}| \approx 0.4,$$

where

$$\epsilon_d = \frac{1}{5} \sum_i \epsilon_{d,i} = 0; \quad \epsilon_p = \frac{1}{3}(\epsilon_{p\sigma} + \epsilon_{p\pi} + \epsilon_{pz})$$

are the centers of "gravity" for the Cu $3d$ and O $2p$ manifolds, respectively. As will be discussed more in detail below (see Sec. VI.E.1) such a parameter choice is confirmed by the corresponding ARPES data^{43,44} giving important information concerning the nonbonding oxygen states. Fig. 2 presents a possible single-hole energy spectrum for a CuO_4 plaquette embedded into an insulating cuprate like $\text{Sr}_2\text{CuO}_2\text{Cl}_2$ calculated with the parameters above. For illustration we show also a step-by-step formation of the cluster energy levels from the bare Cu $3d$ and O $2p$ levels with the successive inclusion of crystalline field (CF) effects, O $2p$ -O $2p$, and Cu $3d$ -O $2p$ covalency.

III. ONE-CENTER FRENKEL-LIKE EXCITONS

Small charge transfer excitons, or excited states arising from the configuration in which an electron is transferred from a negative ion to a nearest neighbor positive ion have been considered many years ago to be the origin of excitonic-like peaks which show up as a low-energy structure of the fundamental absorption band, for instance in alkali halide crystals.⁴⁵ Namely this idea was exploited by Zhang and Ng in their simple model theory of small CT excitons in insulating cuprates.^{19,28} However, in terms of the CuO_4 cluster model the local two-atomic Cu $3d$ -O $2p$ charge transfer generates a number of both intra-cluster and inter-cluster transitions (see Fig. 3). The corresponding electron-hole excitations form small one-

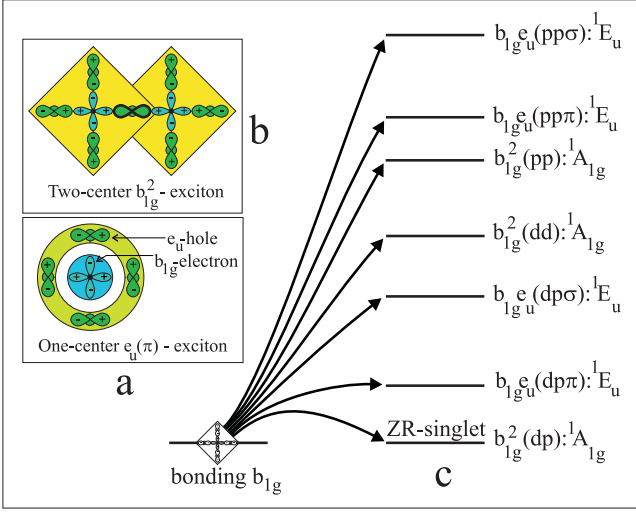


FIG. 3: (a) Simplified illustration of the one-center exciton and (b) the two-center exciton of $b_{1g}^2; pd$, i.e. ZR-singlet type. (c) Classification of the important two-center excitons together with an energy scheme.

and two-center excitons, respectively. The main criteria are the binding energy and the average electron-hole separation. Namely the latter provides the localization and stability of excitations due to their small overlap for nearest neighbors (small tunneling amplitude), and finally leads to a narrow exciton band. Below we address the most probable candidate states for small one- and two-center CT excitons. It should be noted that the main concept which we apply has in many aspects a close similarity with those used for CT excitons of linear-chain organic π -conjugated polymers.^{26,46} Some symmetry aspects of the CT excitons in cuprates were addressed by Cherepanov *et al.*⁴⁷

A. Classification

Among the numerous one-center electron-hole CT excitations the first candidates for dipole-active excitons are CT transitions $b_{1g}^b \rightarrow e_u^{a,b}$ from the ground state b_{1g}^b to the purely oxygen doublet O $2p_\pi$ -O $2p_\sigma$ hybrid states $e_u^{a,b}$, which are allowed in "in-plane" polarization $\mathbf{E} \perp C_4$, and the $b_{1g}^b \rightarrow b_{2u}$ transition to purely oxygen O $2p_z$ -like state, which is allowed in "out-of-plane" polarization $\mathbf{E} \parallel C_4$. All these one-center excitons may be rather simply represented as a hole rotating on the four nearest oxygens around an electron predominantly localized in the Cu $3d_{x^2-y^2}$ state with a minimal electron-hole separation $R_{eh} \approx R_{CuO} \approx 2\text{\AA}$ (see Fig. 3).

The two excitons $b_{1g}^b \rightarrow e_u^b$ and $b_{1g}^b \rightarrow e_u^a$ differ by the oxygen hole density distribution: for the former this has a predominantly O $2p_\pi$ character, while for the latter it has a O $2p_\sigma$ one. It should be noted that the excitonic doublet state may be considered as two currentless states

$e_u(\pm 1)$, or two currentless states $e_u(x, y)$ with quenched orbital motion. The former are excited by circular polarized light, while the latter by linear polarized one. The double degeneracy for the $b_{1g}^b \rightarrow e_u^b$ excitons results in anomalously strong electron-lattice coupling with all features typical for the Jahn-Teller effect,⁴⁸ in particular, high probability to form a self-trapped state. In any case, these excitons should be considered as first candidates for resonant phonon Raman scattering activity. One should specifically emphasize that along with resonance excitation of the allowed Raman modes the Jahn-Teller excitons could generate forbidden phonon modes.

Among dipole inactive excitons one should note $b_{1g}^b \rightarrow b_{2g}$ and, especially, $b_{1g}^b \rightarrow a_{2g}$ with purely oxygen O $2p_\pi$ holes. The latter incorporates a purely oxygen a_{2g} hole, which has in frames of our model the minimal energy among all the purely oxygen states. In accordance with the model energy spectrum (see Ref. 31) its energy should be of the order of $1.5 \div 1.8$ eV, or in other words appears to be lower than the optical gap. This circumstance draws specific attention to this exciton, despite the $b_{1g}^b \rightarrow a_{2g}$ transition is dipole forbidden. Due to the purely oxygen nature of the hole, the $b_{1g}^b \rightarrow a_{2g}$ exciton resembles the dipole active $b_{1g}^b \rightarrow e_u$ exciton, however, contrary to the latter this is a purely O $2p_\pi$ hole.

There are several examples of a qualitative assignment of low-lying optical spectral features to the non-bonding oxygen orbitals, appearing in CuO near 1.7 eV (see Ref. 3,4 and in $\text{Sr}_2\text{CuO}_2\text{Cl}_2$ near 2.5 eV (see Ref. 12). Also, it was shown that the dipole-allowed one-center electron-hole excitation $b_{1g}^b \rightarrow e_u(\pi)$ is visible in the low lying part of the EELS spectrum of $\text{Sr}_2\text{CuO}_2\text{Cl}_2$.³¹ However, to the best of our knowledge, there is at present no unambiguous identification of this one-center excitation (and also of $b_{1g} \rightarrow b_{2u}$) as well-separated entities in 2D insulating cuprates. That is different for 1D cuprates where these one-center excitations built up of non-bonding oxygen-orbitals could be separated in EELS by choosing a momentum transfer perpendicular to the chain direction.³² The conventional one- and two-band Hubbard-like models consider only the Cu $3d_{x^2-y^2}$ and O $2p_\sigma$ orbitals, and do not take into account the nonbonding O $2p_\pi$ and O $2p_z$ orbitals. Partly, that may be justified by the specific properties of the b_{1g} ($d_{x^2-y^2}$) ground state resulting in a predominant contribution of O $2p_\sigma$ orbitals both to the Cu $3d$ - O $2p$ bonding and to the different charge transfer transitions. Optical absorption and EELS activity associated with the nonbonding O $2p_\pi$ and O $2p_z$ orbitals appear to be rather weak if any.

B. Transition matrix elements in optics and EELS

1. Intensities of the electric dipole CT transitions for one-center small excitons

Electric dipole CT transitions for the hole localized in the CuO_4 cluster are allowed from the even ground state b_{1g}^b to the bonding and antibonding purely oxygen odd $e_u^{a,b}$ states for the $\mathbf{E} \perp C_4$ polarization, and to purely oxygen odd b_{2u} state for the $\mathbf{E} \parallel C_4$ one (see Fig. 1). Dipole transition matrix elements for the b_{1g}^b ground state depend essentially on the fact whether the final state is of O $2p_\pi$ or O $2p_\sigma$ character. For the former case we have only a "nonlocal overlap contribution" with two-center integrals

$$\langle b_{1g}^b | qx | e_{ux}(\pi) \rangle = -\langle b_{1g}^b | qy | e_{uy}(\pi) \rangle$$

$$= \cos \alpha_{b_{1g}} \langle d_{x^2-y^2} | qx | e_{ux}(\pi) \rangle$$

$$= q\sqrt{2} \cos \alpha_{b_{1g}} \int \phi_{d_{x^2-y^2}}(\mathbf{r})^* x \phi_{px}(\mathbf{r} - \mathbf{R}) d\mathbf{r};$$

$$\langle b_{1g}^b | qz | b_{2u} \rangle = q\sqrt{2} \cos \alpha_{b_{1g}} \int \phi_{d_{x^2-y^2}}(\mathbf{r})^* z \phi_{pz}(\mathbf{r} - \mathbf{R}) d\mathbf{r}, \quad (3)$$

where $\mathbf{R} \parallel \mathbf{y}$, and

$$\int \phi_{d_{x^2-y^2}}(\mathbf{r})^* x \phi_{px}(\mathbf{r} - \mathbf{R}) d\mathbf{r}$$

$$= - \int \phi_{d_{x^2-y^2}}(\mathbf{r})^* z \phi_{pz}(\mathbf{r} - \mathbf{R}) d\mathbf{r},$$

that results in equal intensities for $b_{1g}^b \rightarrow e_u(\pi)$ and $b_{1g}^b \rightarrow b_{2u}$ transitions. Naturally, that in a more common case we have orthogonalized Wannier functions instead of simple atomic ones, and the calculation of the nonlocal overlap matrix elements is not so straightforward. For the $b_{1g}^b \rightarrow e_u(\sigma)$ dipole transitions to purely O $2p_\sigma$ state we have both nonlocal and local (or "covalent") overlap contributions due to nonzero O $2p_\sigma$ density in the initial b_{1g}^b state

$$\langle b_{1g}^b | qx | e_{ux}(\sigma) \rangle = -\langle b_{1g}^b | qy | e_{uy}(\sigma) \rangle$$

$$= q\sqrt{2} \cos \alpha_{b_{1g}} \int \phi_{d_{x^2-y^2}}(\mathbf{r})^* y \phi_{py}(\mathbf{r} - \mathbf{R}) d\mathbf{r} + \frac{qR_{CuO}}{\sqrt{2}} \sin \alpha_{b_{1g}},$$

where $\mathbf{R} \parallel \mathbf{y}$. It should be noted that namely the local term is the only contribution usually addressed for transition matrix elements.

The bonding and antibonding $e_u^{a,b}$ states incorporate both O $2p_\sigma$ and O $2p_\pi$ orbitals. Therefore, the respective dipole transition matrix elements acquire a rather complex structure. However, for the "covalent", and probably, the leading contribution, we obtain a simple relation

$$\frac{I(b_{1g}^b \rightarrow e_u^b)}{I(b_{1g}^b \rightarrow e_u^a)} = |\tan \alpha_{e_u}|^2 \approx \left| \frac{t_{pp\sigma} + t_{pp\pi}}{\epsilon_{pe_u(\sigma)} - \epsilon_{pe_u(\pi)}} \right|^2. \quad (4)$$

In other words, the relative intensity of the two main electric-dipole transitions is mainly determined by the magnitude of pp -hybridization and does not exceed 0.1 for the typical values of the parameters.

In some cases, it is of practical interest to provide information concerning the allowed dipole transitions between excited states. In our case, these are, first of all, numerous transitions from or to e_u states. For instance, the $a_{2g} \rightarrow e_u^b$ dipole allowed transition has a very large intensity due to a large local contribution to the matrix element:

$$\langle a_{2g} | qx | e_{ux}(\pi) \rangle = \frac{qR_{CuO}}{\sqrt{2}}.$$

It should be noted that the rather simple model of a single CuO_4 cluster allows already to predict both the energies and the relative intensities for such transitions.

2. Intensities of the EELS transitions for one-center small excitons

The intensity of an exciton is determined by the imaginary part of $\epsilon(\mathbf{k}, \omega)$ around a pole, and is given by

$$I \propto k^{-2} |\langle \Psi_{exc} | e^{i\mathbf{k}\mathbf{r}} | \Psi_{GS} \rangle|^2, \quad (5)$$

where Ψ_{exc} is the exciton wave function.²⁸ Within the long-wavelength approximation ($k \rightarrow 0$) the EELS selection rules are the same as in optics if we address the \mathbf{k} direction to be that of the electric field. For the one-center small γ -excitons it is rather easy to obtain the angular \mathbf{k} -dependence of the transition matrix elements in the small \mathbf{k} -approximation:

$$\langle \Psi_{exc} | e^{i\mathbf{k}\mathbf{r}} | \Psi_{GS} \rangle \propto \langle \gamma | e^{i\mathbf{k}\mathbf{r}} | b_{1g}^b \rangle \propto k^L Y_{L\gamma}(\mathbf{k}), \quad (6)$$

where $Y_{L\gamma}(\mathbf{k})$ is a linear superposition of spherical harmonics $Y_{LM}(\mathbf{k})$, which forms a basis of the irreducible representation γ of the D_{4h} point group. We make use of the familiar expansion

$$e^{i\mathbf{k}\mathbf{r}} = 4\pi \sum_{L=0}^{\infty} \sum_{M=-L}^L i^L j_L(kr) Y_{LM}(\mathbf{k}) Y_{LM}^*(\mathbf{r}), \quad (7)$$

restricting ourself to the first nonzero contribution with minimal L . Thus, for different γ one obtains:

$$\langle e_u | e^{i\mathbf{k}\mathbf{r}} | b_{1g}^b \rangle \propto k Y_{1e_u}(\mathbf{k}) \propto k_{x,y}; (\text{dip. approx.})$$

$$\langle a_{1g} | e^{i\mathbf{k}\mathbf{r}} | b_{1g}^b \rangle \propto k^2 Y_{2b_{1g}}(\mathbf{k}) \propto (k_x^2 - k_y^2); (\text{quadr. approx.})$$

$$\langle a_{2g} | e^{i\mathbf{k}\mathbf{r}} | b_{1g}^b \rangle \propto k^2 Y_{2b_{2g}}(\mathbf{k}) \propto k_x k_y; (\text{quadr. approx.})$$

$$\langle b_{1g} | e^{i\mathbf{k}\mathbf{r}} | b_{1g}^b \rangle \propto k^4 Y_{4a_{1g}}(\mathbf{k}) \propto \cos 4\phi; (\text{oct. approx.})$$

$$\langle b_{2g} | e^{i\mathbf{k}\mathbf{r}} | b_{1g}^b \rangle \propto k^4 Y_{4a_{2g}}(\mathbf{k}) \propto \sin 4\phi; (\text{oct. approx.}).$$

Here, ϕ is the azimuthal angle of orientation for the \mathbf{k} vector. In general, among dipole inactive excitons for corner-sharing CuO_4 plaquette systems the a_{1g} and a_{2g} ones are "visible" only along [100] and [110] directions, respectively; the b_{1g}^b exciton is visible both along [100] and [110] directions, while the b_{2g} one does not manifest itself both along [100] and [110] directions. Taking into account only the conventional local overlap ("covalent") contribution to the transition matrix element one may obtain model expressions for $\langle \gamma | e^{i\mathbf{k}\mathbf{r}} | b_{1g}^b \rangle$ suitable throughout the BZ. Thus, one obtains for the O $2p$ local overlap contribution:

$$\langle a_{2g} | e^{i\mathbf{k}\mathbf{r}} | b_{1g}^b \rangle = \langle b_{2g} | e^{i\mathbf{k}\mathbf{r}} | b_{1g}^b \rangle = 0;$$

$$\langle a_{1g}^a | e^{i\mathbf{k}\mathbf{r}} | b_{1g}^b \rangle = -\frac{1}{2} \sin \alpha_{b_{1g}} \cos \alpha_{a_{1g}} \left[\cos \frac{k_x a}{2} - \cos \frac{k_y a}{2} \right];$$

$$\langle b_{1g}^a | e^{i\mathbf{k}\mathbf{r}} | b_{1g}^b \rangle = -\frac{1}{2} \sin \alpha_{b_{1g}} \cos \alpha_{b_{1g}} \left[\cos \frac{k_x a}{2} + \cos \frac{k_y a}{2} \right]; \quad (8)$$

$$\langle e_u^b x | e^{i\mathbf{k}\mathbf{r}} | b_{1g}^b \rangle = \frac{i}{\sqrt{2}} \sin \alpha_{b_{1g}} \sin \alpha_e \sin \frac{k_x a}{2},$$

$$\langle e_u^b y | e^{i\mathbf{k}\mathbf{r}} | b_{1g}^b \rangle = -\frac{i}{\sqrt{2}} \sin \alpha_{b_{1g}} \sin \alpha_e \sin \frac{k_y a}{2};$$

$$\langle e_u^a x | e^{i\mathbf{k}\mathbf{r}} | b_{1g}^b \rangle = -\frac{i}{\sqrt{2}} \sin \alpha_{b_{1g}} \sin \alpha_e \cos \frac{k_x a}{2},$$

$$\langle e_u^a y | e^{i\mathbf{k}\mathbf{r}} | b_{1g}^b \rangle = -\frac{i}{\sqrt{2}} \sin \alpha_{b_{1g}} \cos \alpha_e \sin \frac{k_y a}{2}.$$

For the dipole-allowed $b_{1g} \rightarrow e_u$ transitions the EELS intensity has to decrease in going from the Γ -point to the BZ boundary with

$$\frac{I(\pi/a, \pi/a, 0)}{I(0, 0, 0)} = \frac{I(\pi/a, 0, 0)}{I(0, 0, 0)} = \frac{4}{\pi^2} \approx 0.4.$$

One should note that with the inclusion of the copper contribution the final expression for the matrix element $\langle b_{1g}^a | e^{i\mathbf{k}\mathbf{r}} | b_{1g}^b \rangle$ should be modified

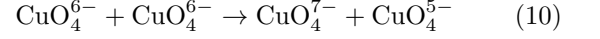
$$\begin{aligned} & \langle b_{1g}^a | e^{i\mathbf{k}\mathbf{r}} | b_{1g}^b \rangle \\ & \approx -\frac{1}{2} \sin \alpha_{b_{1g}} \cos \alpha_{b_{1g}} \left[\cos \frac{k_x a}{2} + \cos \frac{k_y a}{2} - 2 \right]. \quad (9) \end{aligned}$$

Interestingly, that in the frames of the local model for transition matrix elements the a_{2g} and b_{2g} one-center excitons appear to be invisible throughout the BZ body.

IV. TWO-CENTER EXCITONS

A. Electronic structure and classification

Inter-center charge transfer transitions between two CuO_4 plaquettes centered at neighboring sites A and B define two-center excitons in the molecular cluster Cu_2O_7 . These two-center excitons may be considered as quanta of the disproportionation reaction



with the creation of electron CuO_4^{7-} and hole CuO_4^{5-} centers. The former corresponds to completely filled Cu $3d$ and O $2p$ shells, or the vacuum state for holes, while the latter may be found in different two-hole states. These two-hole states can be classified by $\gamma_1 \gamma_2 = \Gamma$ according to the symmetries γ_i of each of the holes. For instance, if we restrict ourselves to charge transfer processes governed by the strongest σ bond, one has to distinguish three different channels b_{1g}^2 , $b_{1g}a_{1g}$ and $b_{1g}e_u$. Only two of them (b_{1g}^2 and $b_{1g}e_u$) have non zero optical matrix elements, but all are important for EELS. Each symmetry different channel contains several wave functions with different Cu and O character (see Section IV.A.1).

To construct ground state and charge transfer excited states we use an approach similar to the well known Heitler-London scheme. In this approach the two hole states for the Cu_2O_7 molecular cluster are formed from different one-center states. We deal with charge states of the CuO_4 plaquette with zero, one, and two holes, respectively, denoted as $\Phi_{A,B}^{(0,1,2)}$. Then, the ground state Ψ_{GS} of the cluster Cu_2O_7 is predominantly given by the symmetrized product of $\Phi_A^{(1)}(b_{1g}^b)\Phi_B^{(1)}(b_{1g}^b)$ coupled to higher states of the same symmetry. Accordingly, the excited (exciton) states are built by product states

$$\phi_{ES}^{eh}(\Gamma) = \Phi_A^{(0)}\Phi_B^{(2)}(\Gamma), \quad (11)$$

with subsequent (anti)symmetrization (see Section IV.A.2).

1. Two-hole configurations for the CuO_4^{5-} center

To classify all two-hole configurations of one CuO_4^{5-} center we use their symmetry $\Gamma = \gamma_1 \gamma_2$ and take into account the Coulomb interaction. The latter is of particular interest both for energetics and the electron structure of two-center excitons. According to symmetry we have to distinguish even Γ configurations (like b_{1g}^2 or $b_{1g}a_{1g}$) and odd Γ configurations (as $b_{1g}e_u$). Alternatively to the notation $\gamma_1 \gamma_2$ we will also use the representations of the D_{4h} symmetry of the CuO_4 cluster (see Ref. 36) with the following correspondence: $b_{1g}^2 = {}^1A_{1g}$ and $b_{1g}e_u = {}^1E_u$. Each channel of two-center excitons, characterized by a $\gamma_1 \gamma_2$ configuration, consists of several wave functions differing by their partial Cu $3d$ and O $2p$ density distribution. These excitons will be denoted by $\gamma_1 \gamma_2$; dd , $\gamma_1 \gamma_2$; pd ,

and $\gamma_1\gamma_2; pp$, respectively. In the sense of quantum chemistry the mixing between several wave functions of one channel can be understood as a configuration interaction effect.

Let us present the simple example of the calculation of the two-hole spectrum in the Zhang-Rice (ZR)-singlet sector²⁴ (i.e. in the b_{1g}^2 -channel). As usually, we assume that the ZR-singlet represents the lowest spin-singlet state formed by the interaction of three "purely ionic" two-hole configurations $|d^2\rangle$, $|pd\rangle$, and $|p^2\rangle$. Here, $|d\rangle = |d_{x^2-y^2}\rangle$ and $|p\rangle = |p_{b_{1g}}\rangle$ are the non-hybridized Cu $3d_{x^2-y^2}$ and O $2p_\sigma$ orbitals, respectively, with bare energies ϵ_d and ϵ_p . Then, the matrix of the full effective Hamiltonian within the bare basis set has a rather simple form

$$\hat{H} = \begin{pmatrix} 2\epsilon_d + U_d & t & 0 \\ t & \epsilon_d + \epsilon_p + V_{pd} & t \\ 0 & t & 2\epsilon_p + U_p^* \end{pmatrix}, \quad (12)$$

where the effective Coulomb parameter for purely oxygen configuration incorporates both the intra-atomic parameter U_p and the oxygen-oxygen coupling to the first and second nearest neighbors, respectively

$$U_p^* = U_p + \frac{1}{4}V_{pp}^{(1)} + \frac{1}{8}V_{pp}^{(2)},$$

and the following condition holds:

$$U_d > U_p > V_{pd}$$

For reasonable values of parameters (in eV): $U_d = 8.5$, $U_p = 4.0$, $V_{pd} = 1.2$, $\epsilon_d = 0$, $\epsilon_p = 3.0$, $t = t_{pd} = 1.3$ (see Ref. 49) we obtain for the ZR-singlet energy $E_{ZR} = 3.6$, and its wave function

$$|\Phi_1^{(2)}\rangle = |b_{1g}^2; pd\rangle = -0.25|d^2\rangle + 0.95|pd\rangle - 0.19|p^2\rangle. \quad (13)$$

It reflects the well-known result that the ZR-singlet represents a two-hole configuration with one predominantly Cu $3d$ and one predominantly O $2p$ hole. The two excited states with energy $E_{ZR} + 5.2$ and $E_{ZR} + 6.7$ eV are described by the wave functions

$$|\Phi_2^{(2)}\rangle = |b_{1g}^2; dd\rangle = 0.95|d^2\rangle + 0.21|pd\rangle - 0.22|p^2\rangle, \quad (14)$$

$$|\Phi_3^{(2)}\rangle = |b_{1g}^2; pp\rangle = -0.17|d^2\rangle - 0.24|pd\rangle - 0.96|p^2\rangle, \quad (15)$$

respectively. Given the ZR-singlet energy one may calculate the transfer energy from b_{1g}^b to the neighboring $b_{1g}^b; pd$ state (the ZR-singlet state), or in short the $b_{1g}^b \rightarrow b_{1g}$ transfer energy:

$$\Delta_{CT} = E_{ZR} - 2E_{b_{1g}} = (3.6 + 0.5)\text{eV} = 4.1\text{eV},$$

where the stabilization energy for the bonding b_{1g}^b state is simply calculated from matrix (12) at $U_d = U_p^* = V_{pd} = 0$. One should note that the minimal $b_{1g}^b \rightarrow b_{1g}$ transfer energy relatively weakly depends on the value of the pd

transfer integral; we obtain the same value 4.2 eV at any value of t between 1.0 ÷ 1.5 eV. This energy depends mainly on the values of $(\epsilon_p - \epsilon_d)$ and V_{pd} .

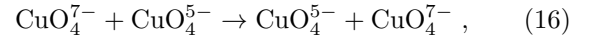
Similar charge transfer energies are obtained in various model approaches. It should be emphasized that this quantity plays a particular role as the minimal charge transfer energy which specifies the charge transfer gap. In the general case it is defined

$$\Delta_{CT} = E_{N+1} + E_{N-1} - 2E_N,$$

as the energy required to remove a hole from one region of the crystal and add it to another region beyond the range of excitonic correlations. The exact diagonalization studies for a series of clusters with different size^{49,50} show that Δ_{CT} strongly diminishes with cluster size from $\approx 4\text{eV}$ for small clusters to $\approx 2.5\text{eV}$ as extrapolated value for large clusters.

2. Ground state and charge transfer excited states of the Cu_2O_7 cluster

As already noted, the states $\Phi_{A,B}^{(0,1,2)}$ of the CuO_4 plaquette centered at A or B will be used to construct the Cu_2O_7 wave functions in a Heitler-London like scheme. Moreover, for two-center molecular clusters like Cu_2O_7 with D_{2h} point symmetry one has two types of excitations: $\phi_{ES}^{eh}(\Gamma) = \Phi_A^0\Phi_B^2(\Gamma)$, and $\phi_{ES}^{he}(\Gamma) = \Phi_A^2(\Gamma)\Phi_B^0$, which differ only by the permutation of electron and hole. These functions will interact due to the resonance reaction



giving rise to the splitting of the two bare excitations discussed in more detail below.

The spin-singlet even ground state for the Cu_2O_7 system can be written as follows

$$\Psi_{GS} = \cos \alpha \phi_{b_{1g}^b b_{1g}^b}^g + \sin \alpha \sum_{\Gamma} a_{\Gamma} \phi_{ES}^g(\Gamma), \quad (17)$$

where $\phi_{b_{1g}^b b_{1g}^b}^g$ is the symmetrized product of the one-center one-hole states $\Phi_A^{(1)}(b_{1g}^b)\Phi_B^{(1)}(b_{1g}^b)$. It is coupled to the even states

$$\phi_{ES}^g(\Gamma) = \frac{1}{\sqrt{2}}(\phi_{ES}^{eh}(\Gamma) \pm \phi_{ES}^{he}(\Gamma)) \quad (18)$$

corresponding to symmetrized (antisymmetrized) bare states $\phi_{ES}^{eh}(\Gamma)$ for even (odd) Γ . Correspondingly, the odd and even excited CT states are given by

$$\Psi_{ES}^u = \sum_{\Gamma} b_{\Gamma} \phi_{ES}^u(\Gamma);$$

$$\Psi_{ES}^g = \cos \alpha \sum_{\Gamma} c_{\Gamma} \phi_{ES}^g(\Gamma) - c_{ES} \sin \alpha \phi_{b_{1g}^b b_{1g}^b}^g, \quad (19)$$

where the index Γ labels different final configurations of the two-hole CuO_4 cluster denoted by $\Gamma = \gamma_1\gamma_2; dd, \gamma_1\gamma_2; pd$, and $\gamma_1\gamma_2; pp$, respectively. In close analogy to (18) we can write

$$\phi_{ES}^u(\Gamma) = \frac{1}{\sqrt{2}}(\phi_{ES}^{eh}(\Gamma) \mp \phi_{ES}^{he}(\Gamma)); \quad (20)$$

for even (odd) Γ .

3. The S - and P -like two-center excitons

The energies of the superposition states (18) and (20) are given by $E_0 \pm |T_{AB}|$, where E_0 is the energy of the bare state $\phi_{ES}^{eh}(\Gamma)$ and T_{AB} is an effective resonance two-particle transfer integral of the resonance reaction (16). The even (odd) states ϕ_{ES}^g (ϕ_{ES}^u) may also be denoted as A_g (B_{1u}) states corresponding to the D_{2h} point symmetry of the Cu_2O_7 cluster. Alternatively, they correspond to S - (for A_g) or P -like (for B_{1u}) two-center excitons. Namely these S - or P -like excitons will draw our main attention below. For brevity, we use the simple g, u labels instead of the A_g, B_{1u} notations.

The different coefficients in (17) and (19) are coupled by normalization and orthogonality conditions like

$$\sum_{\Gamma} |a_{\Gamma}|^2 = \sum_{\Gamma} |b_{\Gamma}|^2 = 1; \quad c_{ES} = \sum_{\Gamma} a_{\Gamma}^* c_{\Gamma}.$$

Its magnitude is actually determined by appropriate hole transfer integrals. It should be noted, however, that our approach is only an approximative one. So, due to the small overlap between the two neighboring CuO_4 plaquettes, the one-hole γ label is likely to be a "bad quantum number". Nevertheless, it can be used in the frames of a semi-quantitative approach. In the single channel approximation where the exciton is dominated by the transfer from b_{1g}^b to one neighboring $b_{1g}\gamma$ state, we may write

$$\sin \alpha = \frac{t_{b_{1g} \rightarrow \gamma}}{\Delta_{b_{1g} \rightarrow \gamma}}, \quad (21)$$

where $t_{b_{1g} \rightarrow \gamma}$ and $\Delta_{b_{1g} \rightarrow \gamma}$ are the CT transfer integral and CT energy, respectively.

Let us note that in our approach the S - and P -excitons are centered at the central oxygen ion of the Cu_2O_7 cluster. That is in contrast to the simple ZN-model²⁸ which implies the hole location on one of the CuO_4 plaquettes. In other words, the ZN-model treats the electrons and holes in the $e-h$ pair substantially asymmetrically, that does not allow to introduce the S - and P -like excitons.

The magnitude of the effective resonance two-particle transfer integral T_{AB} which determines the even-odd splitting is of particular interest in exciton theory. In the real cuprate situation the bare two-center exciton represents a system of two neighboring electron CuO_4^{7-} and hole CuO_4^{5-} centers (given common oxygen). Thus, the resonance reaction corresponds to inter-center transfer of *two holes*, or *two electrons*.

The S -exciton is dipole-forbidden, in contrast to the P -exciton, and corresponds to a so-called two-photon state. However, these two excitons have a very strong dipole-coupling with a large value of the S - P transition dipole matrix element. This points to a very important role played by this doublet in nonlinear optics, in particular in two-photon absorption and third-harmonic generation effects.^{8,16}

The large dipole matrix element between excited S - and P -excitons

$$d = |\langle S | \hat{\mathbf{d}} | P \rangle| \approx 2eR_{\text{CuCu}}, \quad (22)$$

is important for the explanation of the nonlinear optical effects in Sr_2CuO_3 .^{16,18} The magnitude of this matrix element yields a reliable estimate for the effective "length" of the two-center CT exciton.

B. Transition matrix elements for two-center excitons

1. General expressions

In general, the expression for the EELS transition matrix element for two-center excitons has a rather complicated form

$$\begin{aligned} \langle \Psi_{ES}^g | e^{i\mathbf{kr}} | \Psi_{GS} \rangle &= \sin \alpha \cos \alpha \left(-c_{ES} \langle \phi_{b_{1g}^b b_{1g}^b}^g | e^{i\mathbf{kr}} | \phi_{b_{1g}^b b_{1g}^b}^g \rangle + \sum_{\Gamma'} c_{\Gamma}^* a_{\Gamma'} \langle \phi_{ES}^g(\Gamma) | e^{i\mathbf{kr}} | \phi_{ES}^g(\Gamma') \rangle \right), \\ \langle \Psi_{ES}^u | e^{i\mathbf{kr}} | \Psi_{GS} \rangle &= \sin \alpha \sum_{\Gamma'} b_{\gamma}^* a_{\gamma'} \langle \phi_{ES}^u(\Gamma) | e^{i\mathbf{kr}} | \Psi_{ES}^g(\Gamma') \rangle. \end{aligned} \quad (23)$$

It should be emphasized that it is the second term in the ground state wave function (17) which is particularly

important for the local contribution to the transition ma-

trix elements. The different transition matrix elements for the "two-plaquette" Cu_2O_7 system can be easily reduced to "one-plaquette" two-hole matrix elements. One has to use (11) and (18,20) which give $\phi_{ES}^{g,u}(\Gamma)$ as super-

positions of the "one-plaquette" two-hole wave functions $\Phi_{A,B}^{(2)}(\Gamma)$ centered at A and B. Then one finds for the x -axis oriented Cu_2O_7 molecule

$$\begin{aligned}\langle \phi_{ES}^g(\Gamma) | e^{i\mathbf{k}\mathbf{r}} | \phi_{ES}^g(\Gamma') \rangle &= \cos \frac{k_x a}{2} \langle \Phi_A^{(2)}(\Gamma) | e^{i\mathbf{k}\mathbf{r}} | \Phi_A^{(2)}(\Gamma') \rangle, \\ \langle \phi_{ES}^u(\Gamma) | e^{i\mathbf{k}\mathbf{r}} | \phi_{ES}^g(\Gamma') \rangle &= -i \sin \frac{k_x a}{2} \langle \Phi_A^{(2)}(\Gamma) | e^{i\mathbf{k}\mathbf{r}} | \Phi_A^{(2)}(\Gamma') \rangle\end{aligned}\quad (24)$$

for Γ and Γ' of the same parity. Otherwise, the right hand sides in (24) should be interchanged. At the Γ -point $\mathbf{k} = 0$ all these matrix elements are simply reduced to appropriate overlap integrals. The $GS \rightarrow g$ -state transitions at this point are symmetry forbidden, while the $GS \rightarrow u$ -state transitions are allowed in the dipole approximation ($\mathbf{k} \rightarrow 0$). It is of particular importance to note that in accordance with the relations (24) the nonzero dipole response at the Γ -point is derived only from either diagonal "one-plaquette" two-hole matrix elements, or from non-diagonal ones with different parity

of the left and right hand side's functions.

2. Some basic transition matrix elements for CT governed by σ bond

Below we list some nonzero matrix elements for the x -axis oriented two-center S - and P -excitons generated by the main $b_{1g}^b \rightarrow a_{1g}, b_{1g}, e_u$ CT transitions with the strongest σ bonds:

One obtains for the local overlap contribution due to O $2p_\sigma$ states for $\gamma, \gamma' = a_{1g}, b_{1g}$

$$\begin{aligned}\langle \phi_{b_{1g}^b b_{1g}^b}^g | e^{i\mathbf{k}\mathbf{r}} | \phi_{b_{1g}^b b_{1g}^b}^g \rangle &= \rho_{GS}(O2pb_{1g}^b) \cos \frac{k_x a}{2} (\cos \frac{k_y a}{2} + \cos \frac{k_x a}{2}), \\ \langle \phi_{ES}^g(b_{1g}^b \gamma) | e^{i\mathbf{k}\mathbf{r}} | \phi_{ES}^g(b_{1g}^b \gamma) \rangle &= \frac{1}{2} (\rho_{ES}(O2p\gamma) + \rho_{GS}(O2pb_{1g}^b)) \cos \frac{k_x a}{2} (\cos \frac{k_y a}{2} + \cos \frac{k_x a}{2}), \\ \langle \phi_{ES}^g(b_{1g}^b \gamma) | e^{i\mathbf{k}\mathbf{r}} | \phi_{ES}^g(b_{1g}^b \gamma') \rangle &= \frac{1}{2} c_{ES}^*(O2p\gamma) c_{ES}(O2p\gamma') \cos \frac{k_x a}{2} (\cos \frac{k_x a}{2} - \cos \frac{k_y a}{2}), (\gamma' \neq \gamma), \\ \langle \phi_{ES}^u(b_{1g}^b \gamma) | e^{i\mathbf{k}\mathbf{r}} | \phi_{ES}^g(b_{1g}^b \gamma) \rangle &= -\frac{i}{2} (\rho_{ES}(O2p\gamma) + \rho_{GS}(O2pb_{1g}^b)) \sin \frac{k_x a}{2} (\cos \frac{k_y a}{2} + \cos \frac{k_x a}{2}), \\ \langle \phi_{ES}^u(b_{1g}^b \gamma) | e^{i\mathbf{k}\mathbf{r}} | \phi_{ES}^g(b_{1g}^b \gamma') \rangle &= -\frac{i}{2} c_{ES}^*(O2p\gamma) c_{ES}(O2p\gamma') \sin \frac{k_x a}{2} (\cos \frac{k_x a}{2} - \cos \frac{k_y a}{2}), (\gamma' \neq \gamma); \\ \langle \phi_{ES}^g(b_{1g}^b e_u(\sigma)) | e^{i\mathbf{k}\mathbf{r}} | \phi_{ES}^g(b_{1g}^b \gamma) \rangle &= \frac{1}{2} c_{ES}^*(O2pe_u(\sigma)) c_{ES}(O2p\gamma) \sin \frac{k_x a}{2} \sin \frac{k_x a}{2}; \\ \langle \phi_{ES}^u(b_{1g}^b e_u(\sigma)) | e^{i\mathbf{k}\mathbf{r}} | \phi_{ES}^g(b_{1g}^b \gamma) \rangle &= \frac{i}{2} c_{ES}^*(O2pe_u(\sigma)) c_{ES}(O2p\gamma) \sin \frac{k_x a}{2} \cos \frac{k_x a}{2}; \\ \langle \phi_{ES}^g(b_{1g}^b e_u(\sigma)) | e^{i\mathbf{k}\mathbf{r}} | \phi_{ES}^g(b_{1g}^b e_u(\sigma)) \rangle &= \rho_{ES}(O2pe_u(\sigma)) \cos \frac{k_x a}{2} \cos \frac{k_x a}{2};\end{aligned}\quad (25)$$

$$\langle \phi_{ES}^u(b_{1g}^b e_u(\sigma)) | e^{i\mathbf{k}\mathbf{r}} | \phi_{ES}^g(b_{1g}^b e_u(\sigma)) \rangle = -i\rho_{ES}(O2p e_u(\sigma)) \sin \frac{k_x a}{2} \cos \frac{k_x a}{2};$$

and for the local overlap contribution due to Cu $3d_{x^2-y^2}$ states

$$\langle \phi_{b_{1g}^b b_{1g}^b}^g | e^{i\mathbf{k}\mathbf{r}} | \phi_{b_{1g}^b b_{1g}^b}^g \rangle = 2\rho_{GS}(Cu3db_{1g}^b) \cos \frac{k_x a}{2}$$

$$\langle \phi_{ES}^g(b_{1g}^b \gamma) | e^{i\mathbf{k}\mathbf{r}} | \phi_{ES}^g(b_{1g}^b \gamma) \rangle = (\rho_{ES}(Cu3d\gamma) + \rho_{GS}(Cu3db_{1g}^b)) \cos \frac{k_x a}{2},$$

$$\langle \phi_{ES}^u(b_{1g}^b \gamma) | e^{i\mathbf{k}\mathbf{r}} | \phi_{ES}^g(b_{1g}^b \gamma) \rangle = -i(\rho_{ES}(Cu3d\gamma) + \rho_{GS}(Cu3db_{1g}^b)) \sin \frac{k_x a}{2},$$

$$\langle \phi_{ES}^g(b_{1g}^b e_u(\sigma)) | e^{i\mathbf{k}\mathbf{r}} | \phi_{ES}^g(b_{1g}^b e_u(\sigma)) \rangle = \rho_{GS}(Cu3db_{1g}^b) \cos \frac{k_x a}{2}, \quad (26)$$

$$\langle \phi_{ES}^u(b_{1g}^b e_u(\sigma)) | e^{i\mathbf{k}\mathbf{r}} | \phi_{ES}^g(b_{1g}^b e_u(\sigma)) \rangle = -i\rho_{GS}(Cu3db_{1g}^b) \sin \frac{k_x a}{2},$$

$$\langle \phi_{ES}^g(b_{1g}^b \gamma) | e^{i\mathbf{k}\mathbf{r}} | \phi_{ES}^g(b_{1g}^b \gamma') \rangle = \langle \phi_{ES}^u(b_{1g}^b \gamma) | e^{i\mathbf{k}\mathbf{r}} | \phi_{ES}^g(b_{1g}^b \gamma') \rangle = 0, (\gamma' \neq \gamma).$$

Here, $c_{GS,ES}(Cu3d\gamma)$, $c_{GS,ES}(O2p\gamma)$ and $\rho = |c|^2$ are the probability amplitudes and hole densities on copper (oxygen) molecular orbitals for ground, or excited states, respectively. Making use of these expressions we can readily obtain the complete set of EELS transition matrix elements for dipole-allowed and -forbidden two-center excitons. Moreover, they can be used for the description of CT excitons in terms of purely copper $3d\gamma$, or oxygen $2p\gamma$ one-hole states. Namely such an approach could be probably more reasonable in the case of strongly correlated "one-plaquette" two-hole states.

Formulas (23)-(26) clearly show that the simple dipole approximation for EELS transition matrix elements like that one used in the ZN-model^{19,28} cannot satisfactorily describe the \mathbf{k} -dependence of the EELS intensities, and may be misleading. Interestingly, that the oxygen and copper contributions to the local overlap mechanism of EELS transitions have substantially different \mathbf{k} -dependence. So, the O $2p$ contribution to both dipole-allowed and -forbidden transitions for $\gamma, \gamma' = a_{1g}, b_{1g}$ turn to zero at the (π, π) point, contrary to the copper contribution. At this point the active oxygen contribution to the loss function is associated only with dipole-forbidden $\Psi_{GS} \rightarrow \phi_{ES}^g(b_{1g}^b e_u(\sigma))$ transitions. For the [100] direction the oxygen contribution to the EELS intensity for the dipole-allowed transitions decreases twice as faster than the copper one.

In other words, the EELS intensity at the (π, π) point reproduces in such a case the spectral distribution of the two-center excitations generated by the $b_{1g}^b \rightarrow e_u$ CT transition. In contrast, the EELS intensity near the Γ -point, where the S -exciton contribution

turns into zero, reproduces the spectral distribution of the two-center dipole-allowed excitations $g \rightarrow u$, generated by the $b_{1g}^b \rightarrow b_{1g}$ CT transitions both to predominantly oxygen ($4\rho^{ES}(O2p\gamma) > \rho^{ES}(Cu3d\gamma)$) and copper ($4\rho^{ES}(O2p\gamma) < \rho^{ES}(Cu3d\gamma)$) states, as well as the $b_{1g}^b \rightarrow e_u(\pi), e_u(\sigma)$ CT transition to purely oxygen $e_u(\pi), e_u(\sigma)$ states. In principle, this makes it possible to examine the Cu $3d$ and O $2p$ partial composition of the excitons by means of the EELS intensity analysis, though it should be noted that dipole-allowed two-center excitations could interact both with each other and with the dipole-allowed one-center excitations $b_{1g}^b \rightarrow e_u(\pi), e_u(\sigma)$.

3. Transition matrix elements for the b_{1g}^2 -channel of inter-center CT excitons

For illustration, let us consider the b_{1g}^2 -channel of inter-center CT excitons. We have to take into account the admixture of all three singlet wave functions $\Phi_i^{(2)}$ of the ZR-singlet sector ((13)-(15)) to the ground state wave function Ψ_{GS} . The corresponding amplitudes in Eq. (17) will be denoted by $a_{b_{1g}}^{(i)}$. So, the b_{1g}^2 -channel consists of three inter-center CT excitons with energy separations of $\Delta E_{12} \approx 5.2$ eV and $\Delta E_{13} \approx 6.7$ eV, respectively. If we neglect for a moment the configuration interaction effects in the final states, the relative intensities of these three excitons at the Γ -point are given by:

$$|a_{b_{1g}}^{(1)}|^2 : |a_{b_{1g}}^{(2)}|^2 : |a_{b_{1g}}^{(3)}|^2. \quad (27)$$

More accurately, the intensity of the low-energy dipole-allowed two-center exciton with the formation of the ZR-singlet $b_{1g}^2; pd$ is determined by the matrix element:

$$\begin{aligned} \langle \phi_{ES}^u(b_{1g}^2; pd) | e^{i\mathbf{kr}} | \Psi_{GS} \rangle &= -i \sin \alpha \sin \frac{k_x a}{2} \\ &\left[\langle d^2 | e^{i\mathbf{kr}} | d^2 \rangle \left(0.06a_{b_{1g}}^{(1)} - 0.24a_{b_{1g}}^{(2)} + 0.04a_{b_{1g}}^{(3)} \right) \right. \\ &+ \langle pd | e^{i\mathbf{kr}} | pd \rangle \left(0.90a_{b_{1g}}^{(1)} + 0.20a_{b_{1g}}^{(2)} - 0.22a_{b_{1g}}^{(3)} \right) \\ &\left. + \langle p^2 | e^{i\mathbf{kr}} | p^2 \rangle \left(0.04a_{b_{1g}}^{(1)} + 0.04a_{b_{1g}}^{(2)} + 0.18a_{b_{1g}}^{(3)} \right) \right] \quad (28) \end{aligned}$$

where the one-plaquette matrix elements are:

$$\begin{aligned} \langle d^2 | e^{i\mathbf{kr}} | d^2 \rangle &= 2, \\ \langle pd | e^{i\mathbf{kr}} | pd \rangle &= 1 + \frac{1}{2} \left(\cos \frac{k_x a}{2} + \cos \frac{k_y a}{2} \right), \\ \langle p^2 | e^{i\mathbf{kr}} | p^2 \rangle &= \left(\cos \frac{k_x a}{2} + \cos \frac{k_y a}{2} \right). \quad (29) \end{aligned}$$

Let us draw the attention to the different \mathbf{k} dependence of the "diagonal" (the first term) and "non-diagonal" (the second and third terms) contributions to the overall matrix element. When one moves from the Γ -point to (π, π) , the absolute value of the former decreases, contrary to the latter which grows from zero at the Γ -point to a non-zero value at the BZ boundary. The final \mathbf{k} behavior of the overall transition matrix element could be rather complicated depending on the relative signs and magnitudes of the $a_{b_{1g}}^{(i)}$ coefficients, or the admixture amplitudes of the different ZR-singlet-like states in the ground state wave

function. These amplitudes depend mainly on the effective $b_{1g}^b \rightarrow b_{1g}$ transfer integrals for the bare b_{1g}^b hole between two neighboring plaquettes. The parameters suggest the following relationship

$$|a_{b_{1g}}^{(3)}| > |a_{b_{1g}}^{(1)}| > |a_{b_{1g}}^{(2)}|. \quad (30)$$

In other words, the largest effective integrals will be expected for the transfer to predominantly oxygen b_{1g} -like hole states. In such a case, we cannot exclude the appearance of an intensity compensation point due to the competition of the "diagonal" and "non-diagonal" terms in the matrix element. In any case, we may expect a rather unusual \mathbf{k} behavior of the transition matrix element which in turn determines the behavior of the EELS intensity for one of the main low-energy contributions. On the other hand, the large value of $a_{b_{1g}}^{(3)}$ leads to an higher intensity of the high energy CT exciton at the Γ -point in comparison to the low-energy one with an estimated energy separation between the two of ≈ 6.7 eV. All this illustrates the particular importance of the correlation effects for two-hole configurations being the final states for the inter-center CT transitions under consideration. In addition, one should note that a reasonable analysis of the $b_{1g}^b \rightarrow b_{1g}$ channel points to a rather wide spectral range of the intensive two-center CT transitions.

If it were possible to neglect the effects of d^2 - pd - and p^2 -mixing in the b_{1g}^2 configurations, the dipole-allowed b_{1g}^2 -channel could be divided into independent d^2 - pd - and p^2 -contributions with the corresponding EELS intensities $I_{d^2} \propto |\langle d^2 | e^{i\mathbf{kr}} | d^2 \rangle|^2$, $I_{pd} \propto |\langle pd | e^{i\mathbf{kr}} | pd \rangle|^2$, $I_{p^2} \propto |\langle p^2 | e^{i\mathbf{kr}} | p^2 \rangle|^2$ (see the matrix elements from (29)).

The intensities of dipole-forbidden ($g - g$) CT transitions in the b_{1g}^2 -channel turn into zero both at the Γ -point and at the boundary of the Brillouin zone. To illustrate the \mathbf{k} -dependence of the appropriate matrix elements, we restrict ourselves below to the simplified model where only the ZR-singlet contributes to the b_{1g}^2 -channel

$$\langle \phi_{ES}^g(b_{1g}^2; pd) | e^{i\mathbf{kr}} | \Psi_{GS} \rangle = \frac{1}{2} \sin 2\alpha (\rho_{ES}(O2p) - \rho_{GS}(O2p)) \cos \frac{k_x a}{2} \left[\frac{1}{2} \left(\cos \frac{k_x a}{2} + \cos \frac{k_y a}{2} \right) - 1 \right]. \quad (31)$$

It should be noted that for the [11] and [10] directions the matrix element reaches its maximum at $k = \frac{2}{3}k_{max}$. This value depends on the actual difference in the b_{1g} hole density distribution of ground and excited states.

4. Transition matrix elements for the $b_{1g}^b a_{1g}$ -channel of inter-center CT excitons

Taking into account the correlation and configuration interaction effects there appear three $^1B_{1g}$ terms with a

$b_{1g}a_{1g}$ -like configuration which form the final states for the $b_{1g}^b a_{1g}$ -channel of the two-center CT transitions. This channel is only governed by the oxygen contribution, due to the orthogonality of the Cu $3db_{1g}$ and Cu $3da_{1g}$ orbitals. A shorthand analysis of the \mathbf{k} dependence for the different matrix elements listed above in Eqs. (25)-(26) shows that the $b_{1g}^b a_{1g}$ -channel is "silent" both at the Γ -point and all along the (π, π) direction. Along the $(\pi, 0)$ direction we deal with an unusual behavior of the appropriate $P(A_u)$ and $S(A_g)$ excitonic modes. Going to the BZ boundary, the intensity of the former mode increases

while that of the latter one turns into zero both at Γ and at $(\pi, 0)$ with nonzero value in between. So, one may conclude that the $b_{1g}^b a_{1g}$ -channel could be revealed only along the $(\pi, 0)$ direction outside the Γ -point.

5. Transition matrix elements for the $b_{1g}^b e_u$ -channel of inter-center CT excitons

Like the $b_{1g}^b a_{1g}$ -channel the $b_{1g}^b e_u$ -channel is only governed by the oxygen contribution. As it was mentioned above, we have two types of purely oxygen e_u orbitals: $e_u(\sigma)$ and $e_u(\pi)$ with σ and π directions of the O $2p$ lobes, respectively. These orbitals hybridize with each other owing to the O $2p$ -O $2p$ transfer. As a result we obtain four 1E_u terms for the $b_{1g} e_u$ -like two-hole configurations ($b_{1g}^b e_u(\pi)$, $b_{1g}^b e_u(\sigma)$, $b_{1g}^a e_u(\pi)$, $b_{1g}^a e_u(\sigma)$) which form the final state of the $b_{1g}^b e_u$ -channel of the two-center CT transitions.

Non-zero transition matrix elements in Eqs. (25)-(26) are only obtained for the $b_{1g}^b e_u(\sigma)$ -channel. Therefore, the resulting magnitude of the transition matrix elements would be firstly determined by the $e_u(\sigma)$ weight in the $b_{1g} e_u$ configuration for the final 1E_u term. On the other hand, the main contribution to transition matrix elements is determined by the purely oxygen b_{1g} component of the final states. Both these conclusions are of particular importance for the relative intensities in the $b_{1g}^b e_u$ -channel. The doublet of transitions with final anti-bonding b_{1g}^a state is more intensive than the similar doublet with the final bonding b_{1g}^b state: its relative intensity could be estimated to be $|\tan \alpha_{b_{1g}}|^2 \approx 1.3$. For either doublet the strongest intensity is predicted for transitions with final $e_u(\sigma)$ state with estimated relative intensity to be $|\tan \alpha_{e_u}|^2 > 1$.

Different theoretical estimations (see above) point to the predominantly $b_{1g} e_u(\pi)$ structure of the lowest in energy 1E_u term of the two-hole CuO_4^{5-} center, whose separation from the ground state ZR singlet is only about $1.5 \div 2.0$ eV as observed in photoemission experiments⁴³ for $\text{Sr}_2\text{CuO}_2\text{Cl}_2$. Thus, one should expect rather moderate intensities for the appropriate excitonic mode. On the other hand, one might naturally expect a rather strong high-energy transition to the predominantly $b_{1g}^a e_u(\sigma)$ state. Overall, the \mathbf{k} dependence of the transition matrix elements for the $b_{1g}^b e_u$ -channel is rather typical for purely oxygen contributions: the dipole-allowed P modes gradually lose their intensity up to zero going from the Γ -point to the BZ boundary both in (π, π) and $(\pi, 0)$ directions, contrary to the dipole-forbidden S modes, whose intensity rises by approaching the BZ boundary.

It should be noted that the relative energy position of the four CT excitations in the $b_{1g}^b e_u$ -channel is determined by the $e_u(\pi) - e_u(\sigma)$ and the $b_{1g}^b - b_{1g}^a$ separations, which are of the order 5.0 and 6.0 eV, respectively, as predicted by the above quantum-chemical cluster calculations.

V. DYNAMICS AND DISPERSION OF SMALL EXCITONS

A. Rotational and translational motion of two-center excitons

In contrast to one-center Frenkel excitons, the motion of its two-center counterparts is more complicated. We addressed above the internal electron-hole motion resulting in $S - P$ splitting. Now, we consider the rotational and translational motion of two-center excitons. The elongated structure of the two-center exciton results in a set of both rotational and translational modes, depending on the dimension of the lattice of CuO_4 centers. Such modes for the 2D lattice were addressed in the frames of the simple ZN-model:^{19,28} these are rotations of the hole (electron) around the electron (hole) by 90° and 180° , and axial translations (see Fig. 4). Strictly speaking,

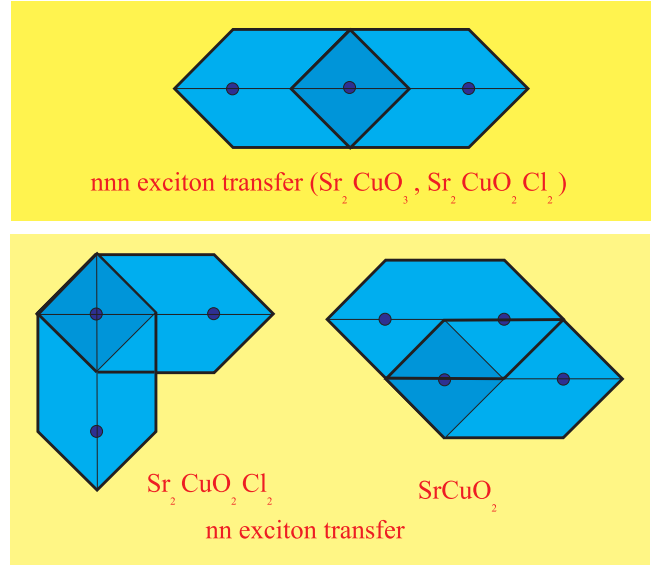


FIG. 4: Different types of next-nearest (nn) neighbor or second nearest neighbor transfer, as well as next-next nearest (nnn) neighbor or 3rd nearest neighbor transfer of two-center excitons.

Zhang and Ng in their simple model considered only the 90° and 180° rotation around the electron center with the respective transfer integrals t_1 and t_4 , and the axial translation accompanied by a 90° rotation around the electron center with transfer integral t_2 .

It is interesting to note that the 90° - and 180° -rotation of the hole around the electron corresponds to the 2nd nearest neighbor and 3rd nearest neighbor hopping of the hole CuO_4^{5-} center which is coupled to a corresponding motion of the electron CuO_4^{7-} center. This problem is closely related to the well-known problem of the ZR-singlet being the ground state of the CuO_4^{5-} center, moving in the lattice formed by the CuO_4^{6-} centers.⁵¹

1. Exciton transfer integrals

Let us consider a three center system ABC and let us compare the collinear 180° geometry with the rectangular 90° one. The exciton transfer integrals between two-center excitons centered at AB or BC, respectively, can be expressed through matrix elements of the effective Hamiltonian H_{eff} that incorporates potential and kinetic energy contributions:

$$\begin{aligned} \frac{1}{2} \langle \Phi_A^{(0)} \Phi_B^{(2)} \pm \Phi_A^{(2)} \Phi_B^{(0)} | \hat{H}_{eff} | \Phi_B^{(0)} \Phi_C^{(2)} \pm \Phi_B^{(2)} \Phi_C^{(0)} \rangle = \\ \pm \frac{1}{2} (T_e^{(2,3)} + T_h^{(2,3)}) + \dots \end{aligned} \quad (32)$$

for diagonal SS and PP transfer, and

$$\begin{aligned} \frac{1}{2} \langle \Phi_A^{(0)} \Phi_B^{(2)} \pm \Phi_A^{(2)} \Phi_B^{(0)} | \hat{H}_{eff} | \Phi_B^{(0)} \Phi_C^{(2)} \mp \Phi_B^{(2)} \Phi_C^{(0)} \rangle = \\ \pm \frac{1}{2} (T_e^{(2,3)} - T_h^{(2,3)}) + \dots \end{aligned} \quad (33)$$

for off-diagonal SP transfer. Here, $T_{e,h}^{(2,3)}$ are the electron (hole) transfer integrals. One has to distinguish the collinear geometry with an exciton transfer to 3rd neighbors $T_{e,h}^{(3)}$ separated by $\approx 4\text{\AA}$, from the rectangular geometry with a transfer to 2nd nearest neighbors $T_{(e,h)}^{(2)}$ separated by $\approx \frac{4}{\sqrt{2}}\text{\AA}$. In (32),(33) we neglected higher order terms which are less important.

According to Eqs. (32),(33) we introduce a set of transfer parameters to describe the exciton dynamics:

$$T_S \approx T_P \approx \frac{1}{2} (T_e^{(3)} + T_h^{(3)}) ,$$

$$T_{SP} \approx \frac{1}{2} (T_e^{(3)} - T_h^{(3)}) ,$$

for the collinear exciton motion, and

$$T_S^{xy} \approx T_P^{xy} \approx \frac{1}{2} (T_e^{(2)} + T_h^{(2)}) ,$$

$$T_{SP}^{xy} \approx \frac{1}{2} (T_e^{(2)} - T_h^{(2)}) ,$$

corresponding to a 90° rotation of the exciton.

All these parameters have a rather clear physical sense. Moreover, the electron (hole) transfer integrals for collinear exciton transfer $T_{e,h}^{(3)}$ are believed to be smaller than $T_{e,h}^{(2)}$ integrals for rectangular transfer. In other words, the two-center excitons prefer to move "crab-like", rather than in the usual collinear mode. This implies a large difference for the excitonic dispersion in [10] and

[11] directions. The electronic wave function in the exciton (contrary to the hole one) has a dominant Cu $3d$ nature that implies a smaller magnitude of the $T_e^{(2,3)}$ parameters compared to the $T_h^{(2,3)}$ ones.

As it was shown by Zhang and Ng,^{19,28} the singlet two-center S, P exciton can move through the antiferromagnetic lattice rather freely in contrast with the single-hole motion. Nevertheless, their values for the second order integrals $t_3 \approx 0.85$ eV and $t_4 \approx 0.65$ eV as derived from an analysis of the experimental EELS data in terms of the simple ZN-model, might be considerably overestimated. As will be seen in the more realistic analysis of EELS data presented below, there are several channels which contribute to the exciton dispersion, such that the numerical values of each of the exciton transfer parameters might be substantially smaller than the effective transfer integrals $t_{1\div 4}$ of the simple ZN-model.

Up to now, we addressed the two-center exciton dynamics in corner-shared systems like Sr_2CuO_3 or $\text{Sr}_2\text{CuO}_2\text{Cl}_2$. However, in 1D systems such as SrCuO_2 there is an additional type of nearest-neighbor transfer of two-center excitons localized on the Cu_2O_7 cluster (as presented in Fig. 4).

2. Tetragonal symmetry and two-center excitons in the 2D CuO_2 layer

The tetragonal symmetry of the 2D CuO_2 layer leads to certain modifications of the results obtained above for excitons in the simple Cu_2O_7 cluster. There, one had to distinguish S - and P -like two-center excitons centered at the common oxygen site, in analogy to the symmetry properties of O $2s$ and O $2p\sigma$ orbitals, respectively. In contrast to that, two-center excitons in the 2D CuO_2 layer could be readily classified with regard to irreducible representations of the tetragonal D_{4h} group. Thus, we can form a set of "large orbital" excitons with A_{1g} , B_{1g} and E_u symmetry (or equivalently with S , D and $P_{x,y}$ symmetry, respectively) rotating around the Cu site (with Cu_5O_{16} geometry). Each two-center exciton classified by the two-hole state Γ of the CuO_4^{5-} center, give rise to one set of 4 excitons.

The symmetry of the excited CT states interacting with the ground state has a crucial influence on the transition matrix elements. So, given the b_{1g} symmetry of the ground hole state in the isolated CuO_4 plaquette, it is the "large orbital" charge transfer state with the same B_{1g} symmetry generated by $S_{x,y}$ two-center transitions that can be mixed with the ground state of the large Cu_5O_{16} cluster. In terms of the 4 small $S_{x,y}, P_{x,y}$ excitons in the 2D elementary cell this corresponds to the mode $S_- = \frac{1}{\sqrt{2}}(S_x - S_y)$. Naturally, the large E_u excitons generated by small $P_{x,y}$ excitons are dipole-allowed, while both A_{1g} and B_{1g} excitons are dipole-forbidden. In terms of the elementary cell modes the dipole-allowed ones are the $P_{x,y}$, or $P_\pm = \frac{1}{\sqrt{2}}(P_x \pm P_y)$ modes.

The mixing of the S_- mode to the ground state in the 2D system defines the intensity of the two-center exciton in the CuO_2 layer, similarly to the simple S_x mode in 1D systems. The transition matrix elements for dipole-allowed excitons in 2D systems is expressed through dipole matrix elements $\langle S_- | \hat{d} | P_{x,y} \rangle$ instead of $\langle S_{x,y} | \hat{d} | P_{x,y} \rangle$ in 1D systems; in other words they would be a factor $\sqrt{2}$ smaller. Thus, the expected intensity of the dipole-allowed two-center CT transitions in 2D system is factor 2 smaller than in 1D systems.

B. The dynamics of two-center excitons in 1D and 2D cuprates

In general, we will consider the two-center Γ -excitons, whose dynamics in frame of the Heitler-London approximation⁵² could be described by an effective one-particle excitonic Hamiltonian with standard form

$$\hat{H}_{exc} = \sum_{\Gamma_1 \Gamma_2 \mathbf{R}_1 \mathbf{R}_2} \hat{B}_{\Gamma_1}^\dagger(\mathbf{R}_1) T_{\Gamma_1 \Gamma_2}(\mathbf{R}_1 - \mathbf{R}_2) \hat{B}_{\Gamma_2}(\mathbf{R}_2) \quad (34)$$

in a site representation with $\hat{B}_{\Gamma_1}^\dagger(\mathbf{R}_1)/\hat{B}_{\Gamma_2}(\mathbf{R}_2)$ being the excitonic creation/annihilation operators, or

$$\hat{H}_{exc} = \sum_{\Gamma_1 \Gamma_2 \mathbf{k}} \hat{B}_{\Gamma_1}^\dagger(\mathbf{k}) T_{\Gamma_1 \Gamma_2}(\mathbf{k}) \hat{B}_{\Gamma_2}(\mathbf{k}) \quad (35)$$

in \mathbf{k} representation. Here the $\Gamma_{1,2}$ indices label different S - or P -excitons. One should note that instead of the S - P manifold we could consider also the dynamics of large orbital excitons with a certain point group symmetry at the Γ -point.

1. The dynamics of isolated SP excitonic doublet in 1D cuprates

We consider the 1D cuprate as a linear chain of corner shared CuO_4 centers directed along the x -axis. The $T(\mathbf{k})$

matrix for an isolated doublet of $S_x = S$ and $P_x = P$ excitons in the 1D cuprate can be written in a rather simple form⁵²

$$T(\mathbf{k}) = \begin{pmatrix} E_S + 2T_S \cos k_x & -2iT_{SP} \sin k_x \\ 2iT_{SP} \sin k_x & E_P + 2T_P \cos k_x \end{pmatrix}. \quad (36)$$

The dispersion of the two-center exciton in 1D system is governed by the nnn exciton transfer. As it was emphasized above, both $(T_S - T_P)$ and T_{SP} are believed to be small that results in the near-degeneracy of the S and P modes with rather trivial dispersion.

The intensity of the dipole-allowed P exciton is expected to decrease sharply with the momentum, while that of the dipole-forbidden S -exciton exhibits a more complicated behavior with zeros at the Γ -point and the BZ boundary, and the maximum midway between the center and the boundary of the zone at $k = 2/3k_{max}$. Overall, one should note that all isolated SP excitonic doublets can manifest a rather small dispersion, however, the \mathbf{k} -dependence of the EELS intensities could be extremely large, and they differ significantly for different transitions. Naturally, in practice one should account for inter-exciton coupling. It is interesting to note that the S - and P -excitons are coupled by dipole transition with large matrix element, which along with the SP degeneracy makes the SP excitonic doublet in 1D cuprates a very promising system for nonlinear optical devices.^{8,16}

2. Dynamics of isolated SP excitonic quartet in 2D cuprates

In the 2D case of an ideal CuO_2 layer we deal with two types of x - (S_x, P_x) and y - (S_y, P_y) oriented S, P excitons in every elementary cell. The $T(\mathbf{k})$ matrix for an isolated quartet of $S_{x,y}$ and $P_{x,y}$ excitons in 2D cuprates can be written by a slight modification of the simple ZN-form²⁸

$$T(\mathbf{k}) = \begin{pmatrix} E_S + 2T_S \cos k_x & -2iT_{SP} \sin k_x & T_S^{xy}(1 + a(k_x, k_y)) & T_S^{xy}(1 + b(k_x, k_y)) \\ 2iT_{SP} \sin k_x & E_P + 2T_P \cos k_x & T_S^{xy}(1 - b(k_x, k_y)) & T_P^{xy}(1 - a(k_x, k_y)) \\ T_S^{xy}(1 + a^*(k_x, k_y)) & T_S^{xy}(1 - b^*(k_x, k_y)) & E_S + 2T_S \cos k_y & -2iT_{SP} \sin k_y \\ T_S^{xy}(1 + b^*(k_x, k_y)) & T_P^{xy}(1 - a^*(k_x, k_y)) & 2iT_{SP} \sin k_y & E_P + 2T_P \cos k_y \end{pmatrix}, \quad (37)$$

where $a(k_x, k_y) = e^{ik_x} + e^{-ik_y}$, $b(k_x, k_y) = e^{ik_x} - e^{-ik_y}$. Here, the two 2×2 blocks on the diagonal are related to S_x, P_x, S_y, P_y excitons, respectively; off-diagonal blocks

describe its coupling. For the $[11]$ direction the exciton transfer matrix breaks up into two similar 2×2 blocks

$$T_{\pm}(\mathbf{k}) = \begin{pmatrix} E_S + 2T_S \cos k_x \pm T_{SS}^{xy}(1 + 2 \cos k_x) & \mp(2iT_{SP} \sin k_x - T_{SP}^{xy}(1 + 2i \sin k_x)) \\ \mp(-2iT_{SP} \sin k_x - T_{SP}^{xy}(1 - 2i \sin k_x)) & E_P + 2T_P \cos k_x \pm T_{PP}^{xy}(1 - 2 \cos k_x) \end{pmatrix}. \quad (38)$$

with basis vectors

$$|S_{\pm}\rangle = \frac{1}{\sqrt{2}}(|S_x\rangle \pm |S_y\rangle); \quad |P_{\pm}\rangle = \frac{1}{\sqrt{2}}(|P_x\rangle \pm |P_y\rangle), \quad (39)$$

respectively. In other words, we have two hybrid S_+P_+ , and two hybrid S_-P_- modes. Generally speaking, all these modes have different energies at $\mathbf{k} = 0$ (the Γ -point). Both hybrid S_-P_- excitons involve the dipole-allowed (for $\mathbf{k} \parallel [11]$) P_- mode and can manifest itself in optical spectra.

In a nearest-neighbor approximation for the exciton transfer, when $T_S = T_P = T_{SP} = 0$, $E_S = E_P$, $T_{SS}^{xy} = T_{PP}^{xy} = T$; $T_{SP}^{xy} = T_1$ we obtain four modes with energies:

$$E_1^{\pm} = E \pm T + [4 \cos^2 k_x (T^2 - T_1^2) + 5T_1^2]^{\frac{1}{2}};$$

$$E_2^{\pm} = E \pm T - [4 \cos^2 k_x (T^2 - T_1^2) + 5T_1^2]^{\frac{1}{2}}$$

and eigenvectors:

$$|(SP)_{\pm}^{(1)}\rangle = e^{i\phi} \cos \alpha |S_{\pm}\rangle + e^{-i\phi} \sin \alpha |P_{\pm}\rangle;$$

$$|(SP)_{\pm}^{(2)}\rangle = e^{i\phi} \sin \alpha |S_{\pm}\rangle - e^{-i\phi} \cos \alpha |P_{\pm}\rangle,$$

where

$$\tan 2\alpha = \frac{T_1[1 + 4 \sin^2 k_x]^{\frac{1}{2}}}{2T \cos k_x}; \quad \tan \phi = 2 \sin k_x.$$

It should be noted that the complex matrix elements in T_{\pm} given $k_x = k_y \neq 0$ evidence the appearance of "twisting" excitonic modes. If we can neglect the nnn electron transfer in comparison with the hole transfer, then we obtain $T = T_1$ and unexpectedly four dispersionless modes with energies:

$$E_1^{\pm} = E \pm T + \sqrt{5}T; \quad E_2^{\pm} = E \pm T - \sqrt{5}T,$$

though the eigenvectors continue to depend on k_x value.

If the electron and hole transfer integrals have the same magnitude ($T_e^{(2)} = T_h^{(2)}$), then $T_1 = 0$ and we obtain pure $|S_{\pm}, P_{\pm}\rangle$ modes with a rather conventional dispersion:

$$E_S^{\pm} = E \pm T(1 + 2 \cos k_x); \quad E_P^{\pm} = E \pm T(1 - 2 \cos k_x).$$

Finally, we address the situation with $T_e^{(2)} = -T_h^{(2)}$, when $T = 0$, and we have two doubly degenerate twisting modes

$$E_1^{\pm} = E + T_1[1 + 4 \sin^2 k_x]^{\frac{1}{2}}; \quad E_2^{\pm} = E - T_1[1 + 4 \sin^2 k_x]^{\frac{1}{2}}$$

with equal weight of S and P modes in eigenvectors.

In frame of the nn-model for the exciton transfer along the [10] direction we address the only example with zero SP -mixing when the exciton dynamics is governed by the only nonzero parameter T . Due to the "crab-like" motion we come to four twisting modes with $S_x - S_y$ and $P_x - P_y$ mixing and energy

$$E_{S_{\pm}} = E_S \pm T[(2 + \cos k_x)^2 + \sin^2 k_x]^{\frac{1}{2}}; \quad E_{P_{\pm}} = E_P \pm |T|.$$

Here, the dipole-allowed P_{\pm} modes appear to be dispersionless. Interestingly to note, that instead of one expected dipole-allowed mode (P_x , or P_y) along this direction, we obtain *two* dipole-allowed modes due to $P_x - P_y$ mixing. Naturally, above we addressed rather simple "toy" models, however, they allow to clearly demonstrate different probable scenarios for the exciton dynamics and its manifestation in optical and EELS spectra.

3. The interaction of two-center excitons in 2D cuprates: The interference effects

Any two excitons of the same symmetry interact with each other. The structure of the interaction matrix for two $S_{x,y}, P_{x,y}$ quartets is similar to (37). The inter-exciton coupling effects its dispersion, and the intensity. The latter is of particular importance for relatively weak transitions in neighborhood of the strong ones. Depending on the phase of the coupling matrix element, the intensity of the definite CT transition can either increase, or decrease due to its interaction with neighbors up to overall suppression. We would like to argue that the particular structure of the interaction matrix elements for the dipole-allowed $P_{x,y}$ excitons makes the appearance of the intensity compensation points a general rule rather than an exception. Indeed, the $P_{x,y} - P'_{x,y}$ coupling is governed by matrix elements $\langle P_{x,y} | T(\mathbf{k}) | P'_{x,y} \rangle \propto \cos k_{x,y}$ that change sign midway between Γ -point and the BZ boundary. The $P_{x,y} - P'_{y,x}$ coupling along the [11] direction is governed by matrix elements $\langle P_{x,y} | T(\mathbf{k}) | P'_{y,x} \rangle \propto (1 - 2 \cos k_{x,y})$ that as well change sign at $k_{x,y} = \frac{1}{3}k_{max}$.

To illustrate inter-exciton coupling effects we address two dipole-allowed two-center excitons, say b_{1g}^2 and $b_{1g}e_u$ type along the [11] direction with the only nonzero $P - P'$ coupling. For simplicity, we assume a conventional bare energy dispersion for both P modes:

$$E(k) = E_P(0) + T_P \cos \frac{k}{\sqrt{2}}$$

with $E_P(0) = 3.1, T_{P'} = 0.4$ eV and $E_{P'}(0) = 4.2, T_P = 0.2$ eV, respectively, and conventional EELS intensity dispersion:

$$I_P(k) = I_P(0) \frac{2 \sin^2 \frac{k}{2\sqrt{2}}}{k^2} (1 + \cos \frac{k}{2\sqrt{2}})^2;$$

$$I_{P'}(k) = I_{P'}(0) \frac{\sin^2 \frac{k}{2\sqrt{2}}}{2k^2}$$

typical for the b_{1g}^2 and $b_{1g}e_u$ -channels, respectively, with intensity ratio like: $I_P(0) : I_{P'}(0) = 1 : 10$. In other words, we have neighboring weak low-energy and strong high-energy excitons. The interaction matrix element is assumed to be

$$\langle P|T(k)|P' \rangle = T_{PP'} (1 - \cos \frac{k}{\sqrt{2}})$$

to provide the non-interacting excitons at the Γ -point. It is easy to see that the noticeable interaction effects manifest itself only in the range $(0.5 \div 1.0)k_{max}$. The sign and magnitude of $T_{PP'}$ were chosen to provide the intensity compensation point near $k = 0.7k_{max}$: $|T_{PP'}| = 0.3$ eV. The Fig. 5 presents the model dispersion curves for the energy (upper panel) together with those for the EELS intensity (lower panel) for two P excitons. We see that the interaction results in a rather weak renormalization of the bare energy dispersion for both excitons. However, the relatively weak interaction leads to a crucial renormalization of the intensity dispersion for weak low-energy exciton with compensation point near $q = 0.7q_{max}$ and blazing up near BZ boundary. The appropriate renormalization for the intensity of the strong high-energy exciton is relatively small. Interestingly to notice that the compensation effect stems from the destructive interference of the two excitons and takes place in a rather narrow momentum range. In experimental spectra this compensation can look like an effect of the "lost" band.

So, we see that the isolated SP excitonic quartets can manifest a rather moderate dispersion, however, the \mathbf{k} -dependence of the EELS intensities is always very strong and differs significantly for different transitions. Overall, the model curves in Fig. 5 clearly demonstrate an extremely important role played by the EELS intensity dispersion. This "matrix element effect", or interference effect is likely to complicate the theoretical treatment of the experimental EELS and RIXS spectra.

4. Two-center excitons in 2D systems as compared with 1D systems

Concluding this subsection we would like to make a short comparative analysis of the main properties of two-center excitons in 2D and 1D systems with corner-shared CuO_4 plaquettes:

1. In 1D system we deal only with nnn exciton transfer, while in 2D system both nnn and nn transfer exists.

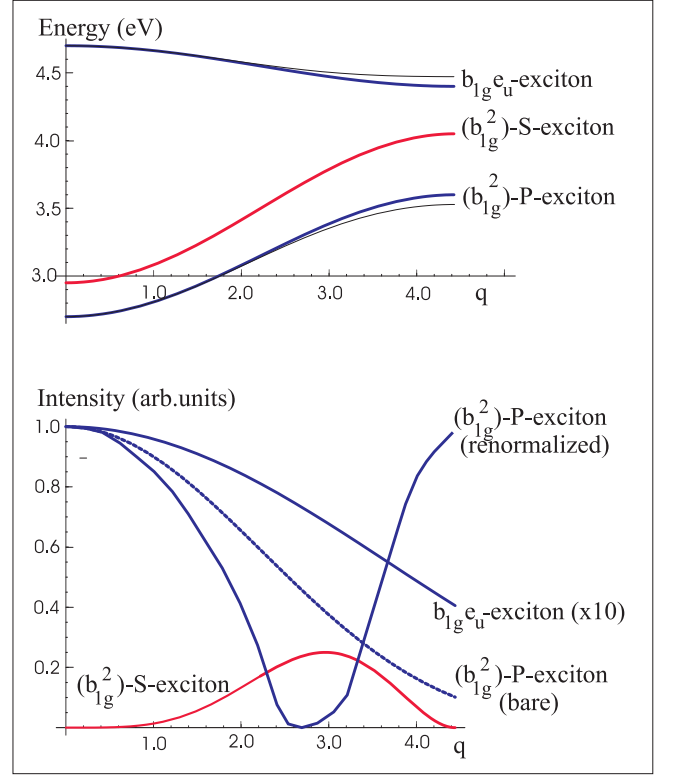


FIG. 5: Model dispersion curves for the energy (upper panel) and the EELS intensity (lower panel) for two neighboring P excitons. For illustration we present the EELS intensity dispersion for isolated S exciton. The momentum dependence of the EELS intensity for b_{1g}^2 - P -exciton demonstrates the destructive interference effect with a full "bleaching" near certain critical q -value. See text for details.

2. At the Γ -point we have in common 2 dipole-allowed transitions associated with one SP excitonic manifold for 2D system contrary to single transition in 1D system.

3. Integral intensity of dipole-allowed transitions associated with one SP excitonic manifold for 2D system two times smaller than in 1D system.

4. The $S - P$ splitting in 1D system is expected to be substantially smaller than in 2D systems. In addition, the $S - P$ dipole matrix elements in 1D system are expected to be as a minimum two times bigger than in 2D systems. Both these quantities essentially determine the magnitude of the third order nonlinear susceptibility $\chi^{(3)}$ and a potential of the system as an optoelectronic material with high performance.¹⁶ Hence, 1D systems should be more effective nonlinear systems as compared with 2D counterparts. Experimental data for 1D Sr_2CuO_3 and 2D $\text{Sr}_2\text{CuO}_2\text{Cl}_2$, and exact diagonalization technique on small clusters confirm this conclusion.^{16,17}

VI. CT EXCITONS IN 0D, 1D, AND 2D INSULATING CUPRATES PROBED BY EELS AND OPTICAL SPECTROSCOPY

By addressing the nature of the electron-hole excitations we should emphasize that a comparative analysis of the optical and EELS spectra in cuprates with different dimensionality of the CuO_4 network is extremely interesting and informative in many respects. In particular, the considerable general interest in comparing the different physical properties of the 0D, 1D and 2D members of the growing cuprate family is warmed up by challenging problems such as the low-dimensional aspect of electronic structure and high- T_c superconductivity.

The 0D cuprates imply a system with well isolated or weakly coupled CuO_4 plaquettes. Such a situation seems to be realized in CuB_2O_4 which belongs to the class of noncentrosymmetric magnetically ordered materials for which the unusual coexistence of weak Dzyaloshinskii-Moriya type ferromagnetism and inhomogeneous (incommensurate) magnetic ordering attracts a lot of attention. CuB_2O_4 crystallizes in the tetragonal space group $I\bar{4}2d$.⁵³ The Cu^{2+} ions at 4b sites are surrounded by four oxygen atoms in planar quadratic coordination so that the local symmetry is $\bar{4}$. The Cu^{2+} ions at 8d sites occupy distorted octahedral positions with an exceptionally large separation of 3.069 Å from the two apical Cu^{2+} ions. Its local symmetry is 2.

Many insulating cuprates represent text-book low-dimensional model systems. The 1D corner-shared ordering of the CuO_4 plaquettes is realized in insulating Sr_2CuO_3 to be the best known model system for a spin-1/2 antiferromagnetic Heisenberg chain and a very promising material for nonlinear optical devices.¹⁶

One of the best representatives for an insulating layered 2D copper oxide might be the oxychloride $\text{Sr}_2\text{CuO}_2\text{Cl}_2$, which is iso-structural to the famous 214 system La_2CuO_4 but contrary to the latter has a single type both of copper and oxygen sites. The compound $\text{Sr}_2\text{CuO}_2\text{Cl}_2$ is one of the most popular model system for the insulating phase of the high- T_c cuprates and 2D spin-1/2 Heisenberg antiferromagnets, and intensively studied both experimentally and theoretically. In this tetragonal antiferromagnet ($T_N \approx 250$ K) with nearly ideal CuO_2 planes there are chlorine atoms instead of apex oxygens with considerably larger $\text{Cu-Cl}_{\text{apex}}$ separation (2.86 Å) than that of $\text{Cu-O}_{\text{apex}}$ (2.42 Å) in La_2CuO_4 . Hence, in $\text{Sr}_2\text{CuO}_2\text{Cl}_2$ one has the opportunity to examine the CuO_2 plane states, both copper and oxygen, without the "parasitic" contribution of apex oxygens. At present, there are a rather large number of experimental data for $\text{Sr}_2\text{CuO}_2\text{Cl}_2$ obtained with the help of optical spectroscopy,¹³ X-ray photoemission (XPS),⁵⁴ ultraviolet photoemission (UPS),⁵⁵ X-ray absorption spectroscopy, (XAS)^{56,57} and angle-resolved photoemission spectroscopy.^{58,59,60,61,62}

The 0D cuprates with isolated CuO_4 plaquettes like Bi_2CuO_4 , the corner-shared and edge-shared 1D chain

cuprates like Sr_2CuO_3 and Li_2CuO_2 , respectively, as well as the 2D systems like $\text{Sr}_2\text{CuO}_2\text{Cl}_2$ should reveal similar signatures of the one-center excitations. However, what concerns the two-center excitations, there appears a principal difference. Naturally, in tetragonal 2D system of corner-shared CuO_4 centers, the two-center excitations manifest itself equally both in a and b in-plane polarizations, while in 1D system of the corner-shared CuO_4 centers they are visible in a similar manner only for "longitudinal" polarization when the electric field is parallel to the chain direction. For the electric field parallel to the CuO_4 plane but perpendicular to the chain direction one might observe only π -like one-center excitations whose intensity is determined by the overlap contribution only. Thus, by comparing the optical response for an idealized 1D chain system with two polarizations we could estimate the contribution of the σ -like two-center excitations by simple subtraction of the two spectra. Naturally, it would be an oversimplification to say that one can deduce the optical response for an idealized 2D plane by simple combination of the 1D spectra with different polarization. A correct extension of the chain data to predict the 2D response should also take into account the additional 90°-coupling of the two-center excitations already at the Γ -point and the more complex dispersion relations. Nevertheless, a simple naive comparative analysis of the chain and plane optical responses could provide important semi-quantitative information on the relative contribution of one- and two-center excitons, their spectral positions, and the relative magnitudes of the overlap and covalent contributions to the dipole matrix elements.

One should note the provisional nature of a certain dimensionality for real cuprates. Even in the so-called 0D systems like CuB_2O_4 , the CuO_4 plaquettes are not really isolated. It might be surprising that among the best candidates for 0D cuprates concerning the optical response are such systems like Li_2CuO_2 or CuGeO_3 . Usually they are considered as 1D systems with edge-sharing CuO_4 plaquettes according to their crystalline structure. For instance, at room temperature, CuGeO_3 belongs to the orthorhombic group D_{2h}^5 ($Pbmm$). The unit cell contains two edge-sharing strongly deformed CuO_6 octahedra, with two types of Cu-O bonds of 2.77 and 1.94 Å, forming one-dimensional antiferromagnetic Cu-O chains along the c axis. However, since the Cu-O-Cu bond angle along the chain is almost 90°, the transfer from one plaquette to its nearest neighbors is strongly suppressed for the in-plane states. Thus, the in-plane charge excitations are localized within one plaquette and with respect to the electronic properties the CuO_4 centers in these compounds can be addressed to be approximately isolated.⁶³ This standpoint is fairly well confirmed in optical and EELS data for Li_2CuO_2 .^{63,64} In what concerns the perpendicular out-of-plane $O\ 2p_z$ orbitals these systems should be considered as typical 1D chain systems with $O\ 2p_\pi$ bonding.

In addition, one should note the problem related to the different symmetry of the crystalline field for the CuO_4

plaquettes in 0D and 2D systems as compared with 1D systems, and between edge-shared and corner-shared 1D systems. For instance, two inequivalent oxygen sites are clearly seen in the polarization-dependent O 1s x-ray absorption spectra for the 1D cuprate Sr_2CuO_3 .⁶⁵ However, the energy separation is found to be as small as 0.5 eV, which is sufficiently smaller than values of the order 1.5 – 2.0 eV, expected from predictions of the simple point-charge model, or LDA calculations.⁶⁵ This experimental finding evidences puzzlingly small non-tetragonal effects near the ground state for the CuO_4 centers in the 1D cuprate Sr_2CuO_3 and allows to make a comparative analysis of the localized excitations with those of the tetragonal 2D cuprate $\text{Sr}_2\text{CuO}_2\text{Cl}_2$. It seems that the internal Cu-O covalent bond for a CuO_4 plaquette provides the main contribution to its electronic structure.

A. The main predictions of the model theory

Before addressing the experimental EELS data we would like to summarize shortly the main results of the model theory of one- and two-center CT excitons in 2D insulating cuprates.

1. One-center excitons

i) We predict three types of dipole-allowed one-center excitons: one exciton b_{2u} with out-of-plane polarization, and two excitons $e_u(\pi)$ and $e_u(\sigma)$ with in-plane polarization and predominantly π and σ O 2p orbital weight, respectively.

ii) The relative value of transition matrix element for the low-energy $e_u(\pi)$ exciton with an estimated energy ≈ 2 eV and for the high-energy $e_u(\sigma)$ exciton is determined by the level of the $\pi - \sigma$ mixing.

iii) The low-energy (near 2 eV) part of the absorption spectrum for a single CuO_4 plaquette is formed by an interplay of forbidden $d - d$ transitions ($b_{1g}^b \rightarrow b_{2g}^b, a_{1g}^b, e_g^b$), forbidden $b_{1g}^b \rightarrow a_{2g}$ and allowed $b_{1g}^b \rightarrow e_u(\pi)$ CT transitions, respectively, which are all close in energy. It is worth noting that for cuprates, as for many other strongly covalent oxides, the conventional division of optical transitions into crystal-field $d - d$ and CT $p - d$ transitions becomes questionable, since the $b_{1g}^b \rightarrow b_{2g}^b, a_{1g}^b, e_g^b$ transitions are accompanied by a strong $p - d$ and $p - p$ charge transfer. The low-energy absorption band is expected to be a result of strong electron-vibrational coupling which lifts the selection rules for certain transitions.

iv) The final $e_u(\pi)$ and $e_u(\sigma)$ states are unstable with respect to the formation of Jahn-Teller (or pseudo-Jahn-Teller) centers with localization of the appropriate CT excitation. This effect is especially important for the $b_{1g}^b \rightarrow e_u(\pi)$ excitation, because the predominant π nature of the hole state results in small transfer integrals and a relatively large effective mass for the exciton. The localization is accompanied by the vibronic reduction of

transition matrix elements. The high-energy $e_u(\sigma)$ exciton is expected to manifest significant intensity both in optical and EELS spectra.

2. Two-center excitons

i) All the two-center excitons generated by the CT governed by the strongest σ bonds can be divided into three channels $b_{1g}^2, b_{1g}a_{1g}, b_{1g}e_u$, respectively, in accordance with the symmetry of the final two-hole state. The main effects in optics and EELS are associated with the b_{1g}^2 - and $b_{1g}e_u$ -channels. In the frame of each channel we deal with different final two-hole states whose energy and wave functions are mainly determined by correlations, or configuration interaction effects. The different theoretical model calculations predict the lowest energy of two-center CT transition for the b_{1g}^2 -channel to be of the order $2 \div 3$ eV.

ii) All the two-center excitons could be divided to even S - and odd P -excitons. For 2D cuprates these excitons generate two sets of four A_{1g}, B_{1g}, E_u plane modes ($S, D, P_{x,y}$ modes).²⁸

iii) The transition matrix elements in optics and EELS have rather complicated \mathbf{k} dependence, substantially differing for the oxygen and copper contributions. The simple dipole approximation fails to explain correctly the \mathbf{k} -dependent effects in EELS.

iv) In frame of the b_{1g}^2 -channel we predict two most important excitons with an energy separation ≈ 7.0 eV. The low-energy exciton with ZR-singlet as a final hole state has rather unusual \mathbf{k} dependence of intensity along the (π, π) direction with a sharp decrease, or even compensation point, by going to the BZ boundary. The high-energy exciton with final ZR-singlet-like $^1A_{1g}$ state of predominantly O 2p nature is likely to manifest the largest intensity for the b_{1g}^2 -channel.

v) In frame of the $b_{1g}e_u$ -channel we predict four most important excitons, generated by CT to $e_u(\pi)$ and $e_u(\sigma)$ orbitals with smaller and larger weight of O 2p _{σ} orbitals, respectively. These weights determine the relative intensities of the appropriate excitons. The photoemission data^{43,44} predict the energy separation between the low-lying $b_{1g}^b \rightarrow e_u(\pi)$ and $b_{1g}^b \rightarrow b_{1g}$ transitions to be of the order 1.5 \div 2.0 eV. The $b_{1g}e_u$ excitons manifest a rather simple dispersion of intensity along both main directions in BZ zone with gradual interchange between dipole allowed and forbidden modes.

3. CT excitons and magnetic subsystem

All parent 1D and 2D copper oxides with corner-shared CuO_4 plaquettes are antiferromagnets with spin-1/2, localized on Cu atoms of the chains or planes, with exchange integral $I \approx 0.1$ eV and a Néel temperature $T_N \sim 300$ K in 2D. So, we have to address the excitons in antiferromagnets. Historically, this problem has been

intensively studied in connection with forbidden $d-d$ excitonic transitions in weakly covalent antiferromagnetic insulators like MnF_2 (see e.g. the paper by Tanabe and Aoyagi in Ref. 66). At first glance, the main allowed electric dipole transitions preserve the spin state and cannot result in conventional or orientational spin fluctuations. On the other hand, the charge transfer transitions are accompanied by a strong spatial redistribution of spin density, and, in a sense, result in a spin density fluctuations. Indeed, the two-center CT exciton is formally associated with spin singlet-singlet transition from a spin-singlet initial state with a *nonzero* spin density on both centers to a spin-singlet final state with a *zero* spin density on both centers. In a sense, this transition is accompanied by a local annihilation of the Néel-like or spin-dimerized state, and the creation of a non-magnetic vacancy. Such a strong spin density fluctuation could result in effective two-magnon (2M) processes. In other words, one might expect strong 2M Raman scattering generated by a two-center exciton. Indeed, the experimental Raman measurements for different insulating cuprates^{10,14} show that the maximal strength of 2M scattering occurs for excitation energies substantially higher than the optical band edge with a peak which we assign to a two-center exciton.

For small one-center excitons we have a rather conventional $s = 1/2 \rightarrow s = 1/2$ transition with spin density fluctuation localized inside the CuO_4 plaquette. Such a transition is not accompanied by strong 2M Raman processes, what could be used to identify such kind of excitons. The redistribution of spin density from the copper atom to the oxygen ones for the $b_{1g} \rightarrow e_u$ transition switches on the strong ferromagnetic Heisenberg O $2p$ -Cu $3d$ exchange with the nearest neighbor CuO_4 plaquettes. Interestingly, the different sign of exchange coupling for e_u and b_{1g} holes with the same neighborhood, ferromagnetic for the former, and antiferromagnetic for the latter, leads to a number of temperature anomalies near the 2D-3D antiferromagnetic phase transition. There is at first the *blue* shift effect for the energy of the small one-center exciton $b_{1g} \rightarrow e_u$ by lowering the temperature near and below T_N . Indeed, at $T \gg T_N$, the average molecular field for the CuO_4 center turns to zero. The 3D antiferromagnetic ordering is accompanied by a rise of exchange molecular fields and respective spin splittings. Due to the different signs of molecular fields for e_u and b_{1g} states this is accompanied by an increase of the transition energy with maximal value of *blue* shift $\Delta \approx \beta(|H_{b_{1g}}| + |H_{e_u}|)$. This quantity could be as large as several tenths of eV. Additionally, one has to expect a strong (of the same order of magnitude) broadening of the excitonic line with increase of the temperature due to strong fluctuations of molecular fields. All these expectations are experimentally found for the 2.0 eV line in $\text{Sr}_2\text{CuO}_2\text{Cl}_2$ ¹² confirming its one-center excitonic nature. A similar situation is observed in La_2CuO_4 ,⁵ although the authors have explained the data by assuming a polaronic nature of electrons and holes with a short-range

interaction in between.

It should be noted that at present there is no relevant theory of spin-excitonic coupling for small CT excitons in strongly covalent and correlated systems. The traditional framework for understanding the two-magnon Raman scattering in antiferromagnets for non-resonant excitation energies has been an effective Loudon-Fleury Hamiltonian,⁶⁷ which implies well localized spins and weak spin-wave like spin fluctuations.

4. CT excitons and phonon subsystem

Generally speaking, the CT exciton creation is usually accompanied by an excitation of lattice modes. Indeed, the hole transfer from Cu $3d$ to O $2p$ state, or from an *ionic* to a *covalent* configuration is accompanied by a significant shortening of the equilibrium Cu-O bond length. The exciton-phonon interaction strongly influences the line-shape of absorption and results in a phonon Raman scattering. The measurement of the Raman intensity as a function of excitation light energy is a very informative probe of the origin of electronic transitions.¹⁰ In particular, this method has allowed⁶ to resolve a fine structure of the low-energy (LE) excitonic feature in La_2CuO_4 with a sharp peak at 2.14 eV as narrow as 50 meV and a broader structure at 1.9 eV. In addition, the authors made the important observation of the selective resonance enhancement, namely that neither the first-order even-parity phonon nor their harmonics show resonant enhancement near the LE exciton peak, while the high-energy (above 450 cm^{-1}) presumably odd Raman modes show large resonant enhancement of as much as a factor of 10 – 40 relative to a laser energy of 2.7 eV. Similar results have been obtained for insulating $\text{YBa}_2\text{Cu}_3\text{O}_{6.1}$.¹⁰ In our opinion, such an unusual behavior of the LE exciton could be associated with its Jahn-Teller nature. Indeed, the $b_{1g} \rightarrow e_u$ transition to the orbital doublet e_u represents a textbook example of a so-called $A - E$ transition.⁴⁸ The excited, orbitally degenerate e_u state is unstable with regard to vibronic coupling with the local distortion modes $A_{1g}, B_{1g}, B_{2g}, E_u$ and the formation of a polaron-like (soliton-like) vibronic center with a complex two- or four-well adiabatic potential and a rather strong renormalization of vibration frequencies. In other words, the doublet e_u state tends to a spontaneous local symmetry breaking, including removal of the inversion center due to interaction with the close in energy even states and pseudo-Jahn-Teller effect. Namely the latter would result in a strong resonance coupling of the $b_{1g} \rightarrow e_u$ exciton with odd E_u lattice modes. Naturally, the structure of such a center would strongly depend on differences in the bare lattice and elastic parameters and differ in 214 and 123 systems. One should emphasize that the formation of the heavy polaron-like, or *localized* small exciton would result in a strong enhancement of its effective mass.

B. Cuprates with well isolated or weakly coupled CuO_4 plaquettes (0D cuprates)

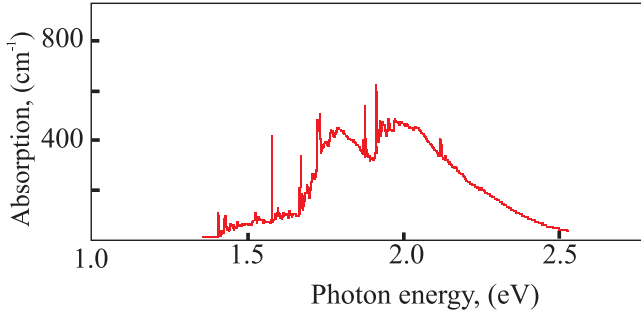


FIG. 6: Low-energy absorption spectra for the 0D cuprate $\text{CuB}_2\text{O}_4(\mathbf{k} \parallel \mathbf{z}, \mathbf{E} \perp \mathbf{z})$.⁶⁸

In Fig. 6 we reproduce the low-energy absorption spectra for the 0D cuprate CuB_2O_4 .⁶⁸ In contrast to most 1D and 2D cuprates where the low-energy absorption bands are broad and featureless, the absorption spectra for the true 0D cuprate CuB_2O_4 (Fig. 6) provide the remarkable opportunity to observe the interplay of low-energy allowed and forbidden transitions. The experimental spectrum shows a number of narrow zero-phonon peaks with up to 70 well-resolved phonon sidebands⁶⁸ imposed on rather broad bands. The former may be assigned to forbidden $b_{1g}^b \rightarrow b_{2g}^b, a_{1g}^b, e_g^b$ ($d-d$) and $b_{1g}^b \rightarrow a_{2g}$ ($p-d$) transitions, while the latter may be assigned to allowed $b_{1g}^b \rightarrow e_u(\pi)$ CT transitions in two types of CuO_4 plaquettes, respectively. The transition energies at Cu_4bO_4 and Cu_8dO_4 plaquettes are similar because of the small influence of the remote apical O^{2-} ions. The experimental EELS spectra for CuB_2O_4 ⁷⁰ exhibit a rather broad dispersionless band peaked near 5 eV which could be associated with a phonon-assisted *localized electron excitation* $b_{1g}^b \rightarrow e_u^a$. The decrease of intensity with the increase of momentum agrees with the cluster (CuO_4) model for electronic states and the dipole nature of transition. A weak feature distinctly observed at small momenta near $2 \div 3$ eV could be assigned to the *localized electron excitation* $b_{1g}^b \rightarrow e_u^b$, i.e. to the low-energy bonding counterpart of e_u state. The optical and EELS spectra for 0D cuprates are governed only by the intra-center transitions.

Interestingly, that very similar EELS spectra are observed in Sr_2CuO_3 for polarization $\mathbf{q} \parallel \mathbf{b}$, that is perpendicular to the chain direction (*out-off-chain* spectra,⁷¹ Fig. 7). Indeed, like for 0D systems, there are no two-center *eh*-excitations governed by strong covalent σ -bonding in this case, and we deal with the predominant contribution of intra-center excitations. So, for the polarization perpendicular to chain direction, the 1D cuprates like Sr_2CuO_3 provide the optical and EELS response typical for a 0D system. Contrary to CuBi_2O_4 , both dipole-allowed $b_{1g}^b \rightarrow e_u^{b,a}$ transitions in Sr_2CuO_3 manifest itself more distinctly with well-defined EELS-peaks at 2.0 and

5.4 eV, respectively. The appropriate peaks in optical conductivity are situated at 1.8 and 4.3 eV, respectively. One should note that these EELS data present a straightforward experimental manifestation of the dipole-allowed intra-center $b_{1g}^b \rightarrow e_u^{b,a}$ excitations without the "parasitic" effect of inter-center transitions.

The situation in 1D systems crucially changes for polarization parallel to the chain direction, or for the *in-chain* spectra. Even in Li_2CuO_2 , where, similarly to real 0D systems, we deal with a predominant contribution of intra-center transitions, the *in-chain* EELS spectra⁶³ look substantially different from those for CuBi_2O_4 . First of all, it concerns the line-shape of the intensive band in the spectral range $4 \div 5$ eV with a very sharp peak at 4.7 eV (Γ -point) and small negative dispersion, which evidences its excitonic nature. Indeed, the concept of the one-center $b_{1g}^b \rightarrow e_u^a$ exciton was successfully applied⁶³ for a quantitative description of these EELS spectra.

Similar absorption spectra as shown in Fig. 6 are also observed in 1D cuprates with 90° Cu-O-Cu bonds like CuGeO_3 .⁶⁹ The EELS spectra of Li_2CuO_2 present another example for the weak energy dispersion of the one-center exciton accompanied by a strong dispersion of its intensity. The different behavior of the one-center dipole-active $b_{1g}^b \rightarrow e_u$ excitations with *in-chain* and *out-off-chain* polarization is straightforwardly associated with specific translational symmetry and lattice dynamics of 1D systems. Indeed, only *in-chain* component of momentum is conserved and can describe the electron and lattice modes. Additionally, the 1D systems are soft with respect to *out-off-chain* distortions that favor the localization of electron excitations. The most probable mechanism governing the structure of the polaron-like one-center exciton in Li_2CuO_2 is associated with strong coupling of the purely oxygen O $2p_\sigma$ hole mode and oxygen distortion modes at the BZ boundary.

C. Polarization dependent EELS spectroscopy of 1D copper oxide Sr_2CuO_3 and separation of one- and two-center CT excitons.

In 2D systems we usually deal with spectra being a hardly resolved superposition of both types of excitons. This renders the separation of transitions with different nature rather difficult. Therefore, there remains still some ambiguity concerning the reliable identification of *two* dipole-allowed one-center CT excitons and *seven* essential two-center CT excitons that might still question its existence as well-defined entities. Unfortunately, this concerns also the structure of the low-energy optical response observed in the spectral range $2 \div 3$ eV, which is of special importance since it is associated with the states which are believed to define the unconventional properties of the cuprates. One should emphasize that conventional optical measurements are restricted only to the Γ -point and cannot separate between localized one-center, dispersionless excitations and two-center excitons with a

noticeable dispersion. In contrast to optics, the angle-resolved EELS spectroscopy provides unique opportunities to reveal the exciton dispersion and separate one- and two-center CT excitons. One-dimensional cuprate compounds are good candidates for such a study since the scattering of electrons with a transferred momentum \mathbf{q} perpendicular to the chain direction excites only electron-hole pairs sitting on one CuO_4 plaquette. On the other hand, for \mathbf{q} parallel to the chain direction, both types of excitons (one- and two-center) can be observed. The interpretation of the EELS spectra with “longitudinal” response were already proposed in terms of the standard one-band Hubbard model.⁷² Below we show that the polarization-dependent angle-resolved EELS study of the 1D cuprate Sr_2CuO_3 with corner-shared CuO_4 plaquettes provides a unique opportunity to separate both the one- and two-center CT excitons, and the two types of one-center excitons, with the first unambiguous manifestation for the relevance of the O $2p_\pi$ holes for the low-energy excitations in cuprates.

The EELS spectra for Sr_2CuO_3 in “longitudinal” response with the transferred momentum oriented along the chain direction were measured earlier on⁷² and have been interpreted within standard Hubbard models. However, such models can describe properly only the “longitudinal” response with the transferred momentum oriented along the chain direction. In this paper we argue that along with the “longitudinal” response a 1D cuprate compound like Sr_2CuO_3 should reveal rather strong low-energy “transversal” response for the transferred momentum oriented in the plane of the CuO_4 plaquettes but perpendicular to the chain direction. The EELS spectra for Sr_2CuO_3 in both polarizations are presented in Fig. 7. Their comparison leads to very important conclusions. As is to be expected, we see a strong difference between the two sets of spectra. First, this concerns the well-defined dispersionless EELS peaks at 2.0 and 5.5 eV in transversal polarization (right hand side panel in Fig. 7). The intensity considerations and the absence of noticeable energy dispersion allow us to associate them with dipole-allowed CT transitions having a particularly localized nature. Moreover, when comparing both spectra we see that despite the strong inequivalence of longitudinal and transversal polarizations in Sr_2CuO_3 the low-energy transition peaked near 2 eV is equally present in both polarizations. Though for longitudinal polarization this is partly hidden for low momentum values by the intensive band peaked at 2.6 eV and is seen as a shoulder, near the BZ boundary it is a well-separated weak band due to the big blue-shift of the intense neighbor. This fact implies that the excitation is localized on the single CuO_4 plaquette being the only common element of longitudinal and transversal geometry in this 1D cuprate with corner-shared CuO_4 plaquettes. Hence, by taking into account the intensity ratio we can unambiguously identify the 2.0 and 5.5 eV peaks in the EELS spectrum of Sr_2CuO_3 with the one-center CT excitons $e_u(\pi)$ and $e_u(\sigma)$, respectively.

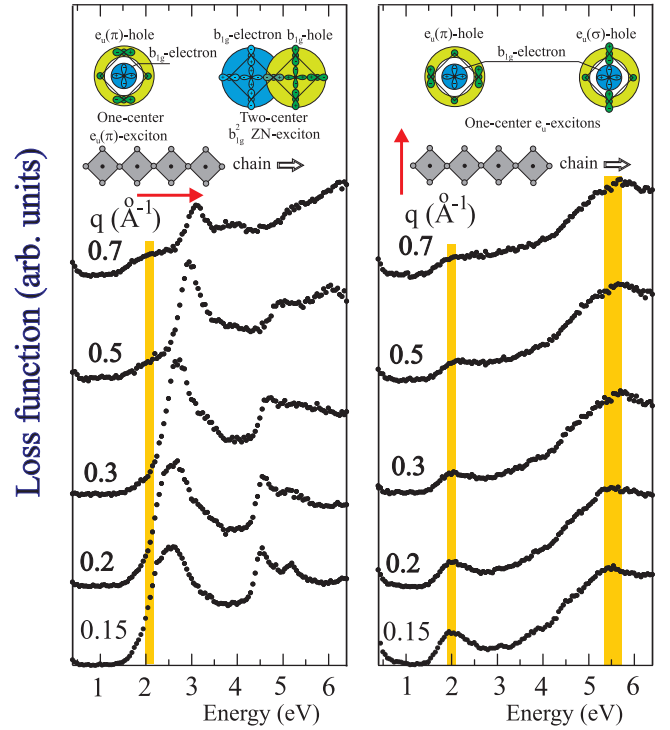


FIG. 7: EELS spectra in Sr_2CuO_3 for longitudinal $\mathbf{q} \parallel \mathbf{a}$ (left panel) and transversal $\mathbf{q} \parallel \mathbf{b}$ (right panel) response with an illustration of one- and two-center excitons.

The sizeable dispersion of the most intense low-lying CT exciton peaked in EELS at 2.6 eV agrees with its two-center nature^{19,28} that is fairly well confirmed in the studies of nonlinear optical effects in Sr_2CuO_3 .^{16,18} Indeed, our analysis of the photoinduced absorption experiments and the measurements of the third-order nonlinear susceptibility $\chi^{(3)}$ in Sr_2CuO_3 ^{16,18} allows to reveal the near-degeneracy of both S - and P -types of two-center CT excitons with an energy of about 2.0 eV, and to obtain a reliable estimate for the transition matrix element (22): $|\langle S | \hat{\mathbf{d}} | P \rangle| \approx 2e \times 4 \text{ \AA}$ (see Fig. 4 in Ref. 18), that straightforwardly points to a two-center CT exciton. In addition, the nonlinear optical response of Sr_2CuO_3 ¹⁸ reveals a weak spectral feature red-shifted to several tenths of eV with regard to the position of the main two-center exciton. It can be attributed to a weak one-center exciton that seems yet to be *invisible* in reflectivity measurements of Sr_2CuO_3 .² In this connection, we would like to emphasize once more the decisive role of *direct* EELS measurements in the observation and unambiguous assignment of one- and two-center excitons in Sr_2CuO_3 as compared with conventional *indirect* optical data.

It is interesting to note that a low-energy transition with small dispersion was also seen in the RIXS data of the 1D cuprate SrCuO_2 published in Ref. 35. In that paper it was interpreted as the onset of the continuum of the one-band Hubbard model. By comparing it with the above discussion of the EELS data of Sr_2CuO_3 we are led to an alternative interpretation of these RIXS data

in terms of a superposition of two different electron-hole excitations, namely the above discussed one- and two-center excitons.

D. CT excitons in 2D insulating cuprates

At first sight, all the above findings are restricted to 1D cuprates. However, already a shorthand inspection of the high-resolution EELS spectra for the 2D system $\text{Sr}_2\text{CuO}_2\text{Cl}_2$ for two polarizations^{20,21} shows nearly the same behavior of the lowest in energy electron-hole excitations. Being encouraged by such an impressive success of our model we can now address the detailed analysis of CT excitons in 2D insulating cuprates.

1. EELS spectra of $\text{Sr}_2\text{CuO}_2\text{Cl}_2$

As it was already noted, $\text{Sr}_2\text{CuO}_2\text{Cl}_2$ is one of the best realizations of a 2D antiferromagnetic, insulating model compound. Of particular importance for the assignment of both one- and two-center excitons are data obtained by ARPES which is a powerful tool to examine the energy spectrum of the two-hole CuO_4^{5-} center. It probes one-particle excitations in contrast to optics and EELS, and the nonbonding oxygen states are clearly visible. At the Γ -point the selection rules for ARPES are the same as for optical and EELS transition, so that ARPES "sees" only the purely oxygen e_u photoholes, or the 1E_u states of the two-hole CuO_4^{5-} center with $b_{1g}e_u$ -like configuration. The inspection of the experimental ARPES spectra for $\text{Sr}_2\text{CuO}_2\text{Cl}_2$ obtained in Refs. 43,44 gives valuable information regarding the two low-lying 1E_u states. It clearly reveals two strong bands separated from the ground state ZR-singlet by $1.5 \div 2.0$ eV and ≈ 5.0 eV, which could be naturally related to the low-energy $e_u(\pi)$ and high-energy $e_u(\sigma)$ photohole states, respectively. Different theoretical estimations^{41,42,73,74,75} corroborate the ARPES data and point to a rather low-energy position of the O $2p_\pi$ states in 1D and 2D cuprates with a corner shared arrangement of CuO_4 plaquettes with $\Delta_{\sigma\pi} = (\epsilon_{p\sigma} - \epsilon_{p\pi}) \approx 1 \div 3$ eV, where $\epsilon_{p\sigma}$ and $\epsilon_{p\pi}$ are the centers of gravity for different O $2p_\sigma$ and O $2p_\pi$ states, respectively.

Unfortunately, the measurements in Ref. 44 are energy restricted and do not provide information regarding the high-energy $b_{1g}e_u(\pi)$ and $b_{1g}e_u(\sigma)$ configurations. However, recent resonant X-ray scattering spectroscopy (RIXS) measurements for different insulating cuprates^{22,23,76} with the incident photon energy tuned to the Cu K edge (hard X-rays) reveal a rather wide ($2 \div 3$ eV) band peaked at $5 \div 6$ eV, which could be unambiguously identified as the band of antibonding Cu $3d$ -O $2p$ ($a_{1g}^a, b_{1g}^a, b_{2g}^a, e_g^a$) states. Hence, the $b_{1g}^b - b_{1g}^a$ separation could be estimated to be ≈ 6.0 eV.

Thus, making use of the ARPES and RIXS data, as well as the theoretical predictions, we can establish an overall picture of optical and EELS spectra (at the Γ -

point). These spectra are governed by dipole-allowed one- and two-center CT excitations and they include:

i) the lowest in energy ($1.5 \div 2.0$ eV) one-center $b_{1g}^b \rightarrow e_u(\pi)$ transition with rather small intensity due to the dominantly O $2p_\pi$ nature of the final state and strong tendency to self-localization (trapping);

ii) the high-energy (≈ 5.0 eV) and rather intensive one-center $b_{1g}^b \rightarrow e_u(\sigma)$ transition;

iii) in frame of the b_{1g}^2 -channel we predict three two-center CT transitions: 1) the rather intensive lowest in energy ($2.0 \div 3.0$ eV) transition with ZR-singlet as a final hole state; 2) the most intensive high-energy transition with ZR-singlet-like final hole state blue-shifted to ≈ 7.0 eV; and 3) probably the less intensive transition blue-shifted to ≈ 5.0 eV with regard to the first one;

iv) in frame of the $b_{1g}e_u$ -channel we predict two doublets of two-center CT transitions shifted ≈ 6.0 eV with regard to each other. The high-energy doublet is relatively more intensive. The partial transitions in both doublets are shifted $3.0 \div 3.5$ eV with regard to each other. Among them, the lowest transition which is rather intense to the $b_{1g}e_u; dp\pi$ state is blue-shifted by $1.5 \div 2.0$ eV with regard to the lowest in energy b_{1g}^2 transition with ZR-singlet as a final hole state, while the more intensive high-energy $b_{1g}e_u; dp\sigma$ transition is blue-shifted by ≈ 5.0 eV with regard to the same transition. In this quartet the most intensive CT transition with $b_{1g}e_u; pp\sigma$ final state is expected to have the maximal energy ($\sim 13 \div 14$) eV among all the CT transitions governed by the strong σ bond.

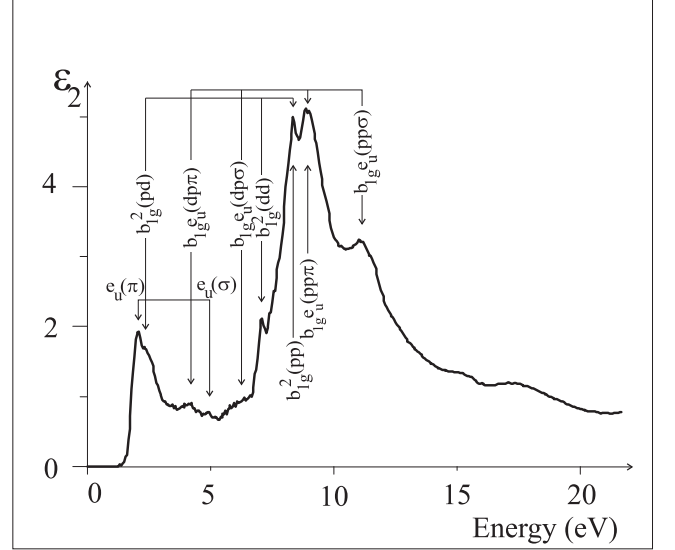


FIG. 8: The spectral dependence of the imaginary part of dielectric function $\epsilon(\omega)$ for $\text{Sr}_2\text{CuO}_2\text{Cl}_2$. Arrows mark the predicted energy position of one-center, two-center b_{1g}^2 -channel, and $b_{1g}e_u$ -channel CT transitions.

As we shall see, all these predictions are in agreement with experimental optical and EELS spectra available for $\text{Sr}_2\text{CuO}_2\text{Cl}_2$.⁷¹

In Fig. 8 we present the spectrum of the imaginary part of dielectric permittivity derived from the Kramers-Kronig transformation of the EELS data.⁷¹ Remarkably, all the excitations which were analysed before correspond to visible features in ϵ_2 . The weak low-energy feature near 2.2 eV in the EELS spectra (2.0 eV in ϵ_2 and optical conductivity) could be ascribed to the lowest in energy one-center $b_{1g}^b \rightarrow e_u(\pi)$ transition. This feature occupies the tail of a rather intensive band peaked at 2.7 eV in EELS spectra (2.4 eV in ϵ_2 and optical conductivity). This band is naturally associated with the lowest in energy $b_{1g}^b \rightarrow b_{1g}$ two-center CT transition with ZR-singlet as a final hole state. Its energy is of particular importance for the whole set of two-center transitions. Having positioned the lowest one- and two-center excitons, the higher states are fixed by the chosen parameter values (see Fig. 2). Two features in EELS, near 4.2 eV and 7.1 eV could be related to two-center $b_{1g}e_u; dp\pi$ and $b_{1g}e_u; dp\sigma$ transitions, respectively, while the wide band near 6.0 eV in EELS could be naturally assigned to the one-center $b_{1g}^b \rightarrow e_u(\sigma)$ transition, whose energy is slightly higher than that of its two-hole counterpart. The overall spectrum of the most effective CT transitions generated by the Cu $3d$ -O $2p$ σ transfer ends with very strong features near $9 \div 10$ and $12 \div 13$ eV in EELS which could be certainly assigned to the high-energy two-center $b_{1g}^2; pp$ CT transition with ZR-singlet-like final hole state of predominantly pp configuration, and the transitions to the $b_{1g}e_u; pp\pi$ and $b_{1g}e_u; pp\sigma$ final states, respectively. All this shows that important spectral information is contained in the range above 8 eV. The peak at about 18 eV is likely to be attributed to transitions with O $2s$ initial state.

The interpretation of EELS spectra for nonzero momentum becomes more complicated due to the energy and intensity dispersion of the dipole-allowed modes and the appearance of numerous new modes which are forbidden at the Γ -point. Hereafter, we focus only on angle-resolved EELS spectra in the spectral range up to 8.0–8.5 eV for several momentum values in [100] and [110] directions, obtained by Wang *et al.*¹⁹ and by Fink *et al.*^{20,21} The spectra differ somewhat by the maximal momenta values and the considerably better resolution in the latter case. For illustration, we reproduce in Fig. 9 the EELS spectra^{20,21} along the [110] direction. The low-energy part of the EELS spectra in the 2D system $\text{Sr}_2\text{CuO}_2\text{Cl}_2$ along the [110] direction and the longitudinal spectra in the 1D system Sr_2CuO_3 have a very similar structure up to some quantitative coincidence. For both compounds the main spectral feature is associated with an intensive band related to the two-center b_{1g}^2 ZN-exciton with clear dispersion peaked at 2.6 eV near the Γ -point and at 3.0 eV near the BZ boundary. In both systems this band has the low-energy shoulder near 2.0 eV which is distinctly seen in the Γ -point or near the BZ boundary. This two-peak structure of the CT band in $\text{Sr}_2\text{CuO}_2\text{Cl}_2$ is corroborated by conventional optical measurements^{12,13} (see Fig. 10). The EELS spectra along the [100] direction manifest

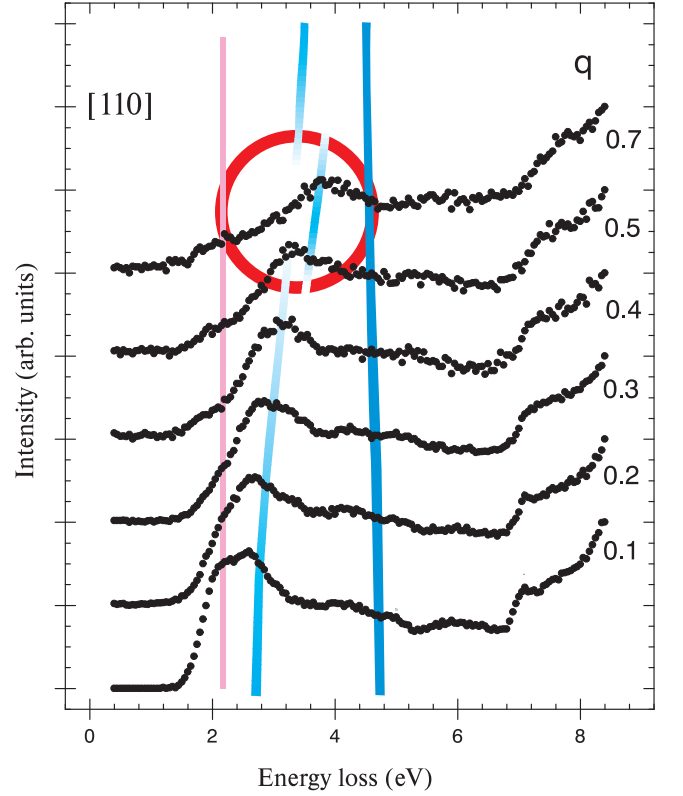


FIG. 9: The spectral dependence of the loss function for $\text{Sr}_2\text{CuO}_2\text{Cl}_2$. The region of possible destructive exciton-exciton interference is highlighted by a circle. See text for details.

an expected overall drop in intensity with relatively small energy dispersion. In contrast to the [100] direction, the main peak for the [110] direction of $\text{Sr}_2\text{CuO}_2\text{Cl}_2$ exhibits clear signatures of strong dispersion, particularly for momentum values in the range $(0.5 \div 0.7)k_{max}$. Namely this effect was a starting point for the model theory of the CT excitons by Zhang-Ng.^{19,28} However, in our opinion, these signatures are not only related to the strong energy dispersion of the ZN-exciton, but also to the unconventional behavior of the intensity dispersion for different excitons with the peculiarities especially in the momentum range $(0.5 \div 1.0)k_{max}$ shown in Fig. 5. Indeed, as it was emphasized above, the intensity of the main peak in the low-energy part of the EELS spectrum for $\text{Sr}_2\text{CuO}_2\text{Cl}_2$, assigned to the dipole-allowed P -exciton associated with the $b_{1g}^b \rightarrow b_{1g}$ two-center CT transition with ZR-singlet as a final hole state, sharply decreases with the increase of momentum along [110] direction with a probable compensation point near the BZ boundary. This circumstance allows to clearly observe a sharp rise of the spectral weight in a rather broad range with the well-defined peak in EELS near 3.8 eV. This spectral feature may be unambiguously associated with the dipole-forbidden A_g counterpart of two-center $b_{1g}e_u; dp\sigma$ exciton, which is allowed and rather intensive at the (π, π) point. Interestingly that the result of this specific behavior of the

EELS intensity for different excitons might be mistaken for manifestation of the energy dispersion of the main peak associated with the $g - u$ dipole-allowed two-center b_{1g}^2 exciton, as it was made by Wang *et al.*¹⁹ Naturally, this mistake leads to a conclusion about very large (~ 1.5 eV) energy dispersion for this exciton. The real energy dispersion for different excitons in our opinion may not exceed the reasonable values of the order of $0.5 \div 1.0$ eV.

Thus, the overall analysis of the experimental EELS spectra in the model 2D insulating cuprate $\text{Sr}_2\text{CuO}_2\text{Cl}_2$ allows us to certainly assign a set of distinctly observed features in a rather wide spectral range $2.0 \div 14.0$ eV to the predicted one- and two-center CT excitons, and confirm the validity of the theoretical concept based on an embedded CuO_4 cluster model.

Interestingly, that the experimental data available allow us to estimate the difference in the $el-h$ -bonding energies E_b for the low-energy one- and two-center CT excitons. Indeed,

$$E_b(e_u(\pi)) - E_b(b_{1g}b_{1g}) = E(^1E_u) - E(^1A_{1g})$$

$$-(E(e_u(\pi)) - E(b_{1g}b_{1g})) \approx (2 \pm 0.5) \text{ eV},$$

where the first term in the right hand side represents the energy of $b_{1g} \rightarrow e_u(\pi)$ excitation in the hole CuO_4^{5-} center with ZR ground state, while the second one represents the difference in the energies of the respective excitons. For the estimate we have made use both of ARPES and EELS data.

2. Fundamental absorption band in parent cuprates: Interplay of one- and two-center CT excitons

A close examination of other materials shows that the two-component structure of the CT gap appears to be a common place for all parent cuprates (see *e.g.*, Refs. 11, 5, and 9). The dipole-allowed localized $b_{1g} \rightarrow e_u^b$ excitation within the CuO_4 plaquette related essentially to the $e_u(\pi)$ state is distinctly seen in optical and EELS spectra for different insulating cuprates as a separate weak feature or a low-energy shoulder of the more intensive band near 2.5 eV assigned to the inter-center CT transition associated with the Zhang-Rice singlet-like excitation $b_{1g}^2; pd$.

Both components are characterized by a different coupling to the magnetic and phonon subsystems thus providing additional ways to separate them. For small one-center excitons we have a rather conventional $s = 1/2 \rightarrow s = 1/2$ transition with a spin density fluctuation localized inside the CuO_4 plaquette. In contrast to the two-center spin-singlet excitation, such a transition is not accompanied by strong two-magnon Raman processes, what could be used to identify this kind of exciton. The redistribution of spin density from copper to oxygen for the $b_{1g} \rightarrow e_u$ transition switches on a strong ferromagnetic Heisenberg exchange between nearest neighbor

CuO_4 plaquettes. The different sign of exchange coupling for the e_u and the b_{1g} holes (ferromagnetic for the former, and antiferromagnetic for the latter) leads to a number of temperature anomalies near the antiferromagnetic phase transition. First, one expects a line broadening and a *blue* shift for the energy of the one-center exciton $b_{1g} \rightarrow e_u$ by lowering the temperature near and below T_N . All these expectations are experimentally found for the 2.0 eV line in $\text{Sr}_2\text{CuO}_2\text{Cl}_2$ ¹² confirming its one-center CT excitonic nature.

The behavior of one- and two-center excitons in monoxide CuO ^{3,4} has some specific features due to the low (monoclinic) crystal symmetry. The $e_u(\pi)$ state is splitted into two components with markedly differing inter-chain $e_u(\pi) - b_{1g}$ exchange, and the respective CT bands near 1.7 eV show markedly different temperature behaviors.⁴ Some experimental data which demonstrate the two-peak structure of the CT gap in insulating cuprates are presented in Fig. 10.

VII. CONCLUSION

We have developed a semi-quantitative cluster approach based on the complete Cu $3d$ -O $2p$ set of the embedded CuO_4 cluster orbitals with a reasonable choice of single-particle and correlation parameters to consistently describe the electron-hole excitations in insulating cuprates in a rather wide energy range up to $10 \div 15$ eV. We extended the Zhang-Ng model by considering the complete set of Cu $3d$ and O $2p$ orbitals and by introducing one-center and two-center excitons. In this connection, it is worth noting that the small charge transfer exciton of the ZN-model can actually be attributed namely to one-center excitons rather than to two-center ones (see *e.g.*, Fig. 3 in Ref. 28). Instead of one $d - p_\sigma$ CT transition of the ZN-model with an energy ≈ 2.5 eV (Γ -point) we arrive at a set of one- and two-center excitons generated by $d - p_\sigma$ charge transfer, and occupying a very broad energy range from ≈ 2 up to ≈ 13 eV. Moreover, the largest dipole intensities have the excitons with the highest energy $9.0 \div 13.0$ eV.

The simple cluster model allows to consistently account for correlation effects in the final two-hole states for two-center excitons. It is shown that these effects are of particular importance both for the energies and intensities of such excitons.

We argue of an important role played by the transition matrix element effects both in optical and EELS spectra. In the latter case we obtain the momentum dependence of matrix elements for different both intra-center and inter-center transitions. One should note that the optical and EELS measurements provide a very important instrument to inspect the electronic structure and the energy spectrum of insulating cuprates. However, decisive conclusions might be taken only after a detailed account for "matrix element" or intensity effects.

The exciton-exciton interaction is shown to be of par-

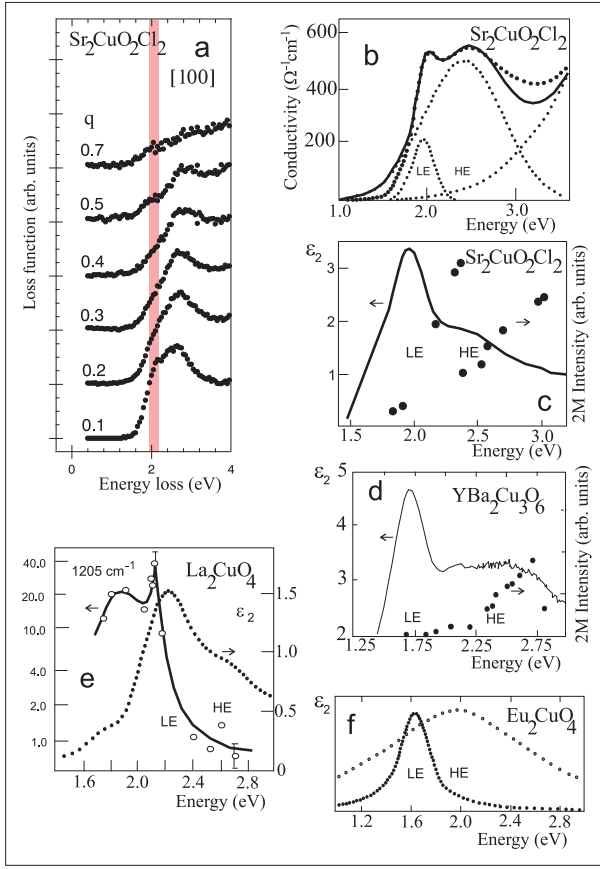


FIG. 10: Some experimental results of EELS and optical measurements for different insulating cuprates which clearly demonstrate a structure of the optical gap: a) low-energy part of EELS spectra in $\text{Sr}_2\text{CuO}_2\text{Cl}_2$ for $\mathbf{k} \parallel [100]$ ⁷¹; b) optical conductivity in $\text{Sr}_2\text{CuO}_2\text{Cl}_2$ ¹²; c), d) imaginary part of the dielectric response in $\text{Sr}_2\text{CuO}_2\text{Cl}_2$ ^{13,14} and $\text{YBa}_2\text{Cu}_3\text{O}_6$,¹¹ respectively, together with the integrated intensity of the related two-magnon (2M) Raman spectrum as a function of the laser excitation energy; e) imaginary part of the dielectric response in La_2CuO_4 ⁵ and the normalized integrated intensity of 1205 cm^{-1} Raman line in La_2CuO_4 as a function of the laser excitation energy;⁶ f) contribution of two fitted oscillators to the imaginary part of the dielectric function for the insulating Eu_2CuO_4 .⁹

particular importance for the actual momentum dependence of the EELS intensities being a probable origin of such peculiarities as an intensity compensation point due to a destructive exciton-exciton interference.

Starting from the predictions of the model theory and some ARPES data we were able to give a semi-quantitative description of the experimental EELS spectra for $\text{Sr}_2\text{CuO}_2\text{Cl}_2$ that is free from many shortcomings of the simplified ZN-model. Both, the different experimental data and the theoretical analysis show that the nature of the CT gap in insulating parent cuprates is determined by two nearly degenerate excitations, a localized intra-center and a inter-center CT exciton with considerable dispersion. The former represents the op-

tical counterpart of the so-called "1 eV peak" revealed by ARPES measurements in a number of cuprates and is associated with the hole CT transition $b_{1g} \rightarrow e_u(\pi)$ from the Cu $3d$ -O $2p$ hybrid $b_{1g} \propto d_{x^2-y^2}$ state to the purely oxygen O $2p_\pi$ state localized on the CuO_4 plaquette, while the latter corresponds to the $b_{1g}^b \rightarrow b_{1g}$ CT transition between neighboring plaquettes with the ZR singlet being the final two-hole state.

Making use of the EELS measurements for the 1D cuprate Sr_2CuO_3 with two different directions of the transferred momentum, we demonstrate straightforwardly the two-peak nature of the CT gap with the co-existence of nearly degenerate one- and two-center CT excitons. In contrast to the 2D case, the two different types of excitons may be well separated by choosing the transferred momentum to be perpendicular to the chain direction.

The structure of the optical gap with two rather well-defined CT excitons seems to be typical for a wide group of parent cuprates that implies a revisit of some generally accepted views on the electronic structure both of 1D and 2D cuprates.

The nonbonding O $2p_\pi$ states with e_u and a_{2g} symmetry form the energetically lowest purely oxygen hole states localized on a CuO_4 plaquette with energy ≈ 2 eV. One might speculate that these O $2p_\pi$ states could be as preferable for the localization of additive hole as the $b_{1g} \propto d_{x^2-y^2}$ ground state which would result in the instability of the Zhang-Rice singlet in doped cuprates. The most probable candidate states for a competition in energy with the Zhang-Rice (b_{1g}^2) (or $^1A_{1g}$) singlet are the singlet 1E_u , or the triplet 3E_u terms of the $b_{1g}e_u$ configuration. Such a $^1A_{1g} - ^1,^3E_u$ competition for the hole-doped CuO_4 plaquette can result in an unconventional behavior of doped cuprates. Perhaps, this could substantially influence the nature of the superconducting state in these systems. Such a conclusion is supported both by local-density-functional calculations,^{41,73} *ab initio* unrestricted Hartree-Fock self-consistent field MO method (UHF-SCF) for copper-oxygen clusters,^{74,75} and a large variety of experimental data. To the best of our knowledge, one of the first quantitative conclusions on a competitive role of the hybrid copper-oxygen $b_{1g}(d_{x^2-y^2})$ orbital and purely oxygen O $2p_\pi$ orbitals in the formation of valence states near the Fermi level in the CuO_2 planes has been made by A.K. McMahan *et al.*⁷³ and J. Tanaka *et al.*⁷⁴ Namely these orbitals, as they state, define the low-energy physics of copper oxides.

Insulating 2D cuprates like $\text{Sr}_2\text{CuO}_2\text{Cl}_2$ are not molecular crystals, and making use of the small exciton approach inevitably leads to problems with strong excitonic overlap and mixing, and manifestation of band-like effects owing to electron-hole pair decoupling. Nevertheless, we suppose that the strong electron-lattice polarization effects⁴⁵ for CT states may provide an effective localization of CT excitons. So, the small exciton model turns out to be a good and instructive approximation to describe optical and EELS spectra in different insulating

cuprates with CuO_4 plaquettes. In this connection, we would like to emphasize the specific role played by the ground state of the cuprate in the formation of optical and EELS response. For a strongly correlated ground state the main part of the optical and EELS response intensity is determined by the excitonic sector, while for a band-like weakly correlated ground state it is the sector of unbound electron-hole pairs. Moreover, in the case of the strongly-correlated insulating cuprates it seems misleading to search for separate contributions of excitons and electron-hole continuum.²⁸

Concluding, it should be noted that the quantum-chemical CuO_4 cluster model represents a physically clear albeit rather simplified approach to consider electron-hole excitations. However, it seems that such an ap-

proach allows to catch the essential physics of the charge transfer transitions, and should be a necessary step both in the qualitative and semi-quantitative description of insulating cuprates.

VIII. ACKNOWLEDGMENTS

A.S.M. acknowledges the stimulating discussions with B.B. Krichevstov, R.V. Pisarev, N.N. Loshkareva, Yu.P. Sukhorukov, and support by SMWK Grant, INTAS Grant No. 01-0654, CRDF Grant No. REC-005, RFBR Grant No. 04-02-96077. S.-L.D. and J.M. acknowledge the support by DFG.

-
- ¹ T. Zaanen, G.A. Sawatzky, and J.W. Allen, *Phys. Rev. Lett.* **55**, 418 (1985).
 - ² M. Imada, A. Fujimori, and Y. Tokura, *Rev. Mod. Phys.* **70**, 1039 (1998).
 - ³ A.S. Moskvin, N.N. Loshkareva, Yu.P. Sukhorukov, M.A. Sidorov, and A.A. Samokhvalov, *Zh. Eksp. Teor. Fiz.* **105**, 967 (1994) [*JETP*, **78**, 518 (1994)].
 - ⁴ Yu.P. Sukhorukov, N.N. Loshkareva, A.A. Samokhvalov, and A.S. Moskvin, *Zh. Eksp. Teor. Fiz.* **108**, 1821 (1995) [*JETP*, **81**, 998 (1995)].
 - ⁵ J.P. Falck, A. Levy, M.A. Kastner, and R.J. Birgeneau, *Phys. Rev. Lett.* **69**, 1109 (1992).
 - ⁶ I. Ohana, D. Heiman, M.S. Dresselhaus, and P.J. Picone, *Phys. Rev. B* **40**, 2225 (1989).
 - ⁷ H. Kishida, M. Ono, A. Sawa, M. Kawasaki, Y. Tokura, and H. Okamoto *Phys. Rev. B* **68**, 075101 (2003).
 - ⁸ A. Schülzgen, Y. Kawabe, E. Hanamura, A. Yamanaka, P.-A. Blanche, J. Lee, H. Sato, M. Naito, N.T. Dan, S. Uchida, Y. Tanabe, and N. Peyghambarian, *Phys. Rev. Lett.* **86**, 3164 (2001).
 - ⁹ B.B. Krichevstov, R.V. Pisarev, A. Burau, H.-J. Weber, S.N. Barilo, and D.I. Zhigunov, *J. Phys.: Cond. Mat.* **6**, 4795 (1994).
 - ¹⁰ E.T. Heyen, J. Kircher, and M. Cardona, *Phys. Rev. B* **45**, 3037 (1992-II).
 - ¹¹ S.L. Cooper, D. Reznik, and A. Kotz *et al.*, *Phys. Rev. B* **47**, 8233 (1993).
 - ¹² H.S. Choi, Y.S. Lee, T.W. Noh, E.J. Choi, Yunkyu Bang, and Y.J. Kim, *Phys. Rev. B* **60**, 4646 (1999).
 - ¹³ A. Zibold, H.L. Liu, S.W. Moore, J.M. Graybeal, and D.B. Tanner, *Phys. Rev. B* **53**, 11734 (1996).
 - ¹⁴ G. Blumberg, P. Abbamonte, M. V. Klein, W.C. Lee, D.M. Ginsberg, L.L. Miller, and A. Zibold, *Phys. Rev. B* **53**, R11930 (1996).
 - ¹⁵ A.B. Schumacher, J.S. Dodge, M.A. Carnahan, R.A. Kaindl, D.S. Chemla, and L.L. Miller, *Phys. Rev. Lett.* **87**, 127006 (2001).
 - ¹⁶ T. Ogasawara, M. Ashida, N. Motoyama, H. Eisaki, S. Uchida, Y. Tokura, H. Ghosh, A. Shukla, S. Mazumdar, and M. Kuwata-Gonokami, *Phys. Rev. Lett.* **85**, 2204 (2000).
 - ¹⁷ Y. Mizuno, K. Tsutsui, T. Tohyama, and S. Maekawa, *Phys. Rev. B* **62**, R4769 (2000-II).
 - ¹⁸ H. Kishida, H. Matsuzaki, H. Okamoto, T. Manabe, M. Yamashita, Y. Taguchi, and Y. Tokura, *Nature* **405**, 929 (2000).
 - ¹⁹ Y.Y. Wang, F.C. Zhang, V.P. Dravid, K.K. Ng, M.V. Klein, S.E. Schnatterly, and L.L. Miller, *Phys. Rev. Lett.* **77**, 1809 (1996).
 - ²⁰ R. Neudert, T. Boeske, O. Knauff, M. Knupfer, M.S. Golden, G. Krabbes, J. Fink, H. Eisaki, and S. Uchida, *Physica B* **230-232**, 847 (1997).
 - ²¹ J. Fink, R. Neudert, H.C. Schmelz, T. Boeske, O. Knauff, S. Haffner, M. Knupfer, M.S. Golden, G. Krabbes, H. Eisaki, and S. Uchida, *Physica B* **237-238**, 93 (1997).
 - ²² P. Abbamonte, C.A. Burns, E.D. Issacs, P.M. Platzman, L.L. Miller, S.W. Cheong, and M.V. Klein, *Phys. Rev. Lett.* **83**, 860 (1999).
 - ²³ M.Z. Hasan, E.D. Issacs, Z.-X. Shen, L.L. Miller, K. Tsutsui, T. Tohyama, and S. Maekawa, *Science*, **288**, 1811 (2000); M.Z. Hasan, E.D. Issacs, Z.-X. Shen, and L.L. Miller, *cond-mat/0102492*.
 - ²⁴ F.C. Zhang and T.M. Rice, *Phys. Rev. B* **37**, 3759 (1988).
 - ²⁵ J. Wagner, W. Hanke, and D.J. Scalapino, *Phys. Rev. B* **43**, 10517 (1991).
 - ²⁶ D. Guo, S. Mazumdar, S.N. Dixit, F. Kajzar, F. Jarka, Y. Kawabe, and N. Peyghambarian, *Phys. Rev. B* **48**, 1433 (1993-I).
 - ²⁷ M.E. Simon, A.A. Aligia, C.D. Batista, E.R. Gagliano, and F. Lema, *Phys. Rev. B* **54**, R3780 (1996-II); M.E. Simon, A.A. Aligia, and E.R. Gagliano, *cond-mat/9707128*.
 - ²⁸ F.C. Zhang and K.K. Ng, *Phys. Rev. B* **58**, 13520 (1998).
 - ²⁹ Eiichi Hanamura, Nguen Trung Dan, and Yukito Tanabe, *Phys. Rev. B* **62**, 7033 (2000).
 - ³⁰ R.O. Kuzian, R. Hayn, and A.F. Barabanov, *Phys. Rev. B* **68**, 195106 (2003).
 - ³¹ A.S. Moskvin, R. Neudert, M. Knupfer, J. Fink, and R. Hayn, *Phys. Rev. B* **65**, 180512(R) (2002).
 - ³² A. S. Moskvin, J. Málek, M. Knupfer, R. Neudert, J. Fink, R. Hayn, S.-L. Drechsler, N. Motoyama, H. Eisaki, and S. Uchida, *Phys. Rev. Lett.* **91**, 037001 (2003).
 - ³³ W. Stephan and K. Penc, *Phys. Rev. B* **54**, R17 269 (1996); K. Penc and W. Stephan, *Phys. Rev. B* **62**, 12 707 (2000).
 - ³⁴ K. Tsutsui, T. Tohyama, and S. Maekawa, *Phys. Rev. B* **61**, 7180 (2000).
 - ³⁵ Y.-J. Kim, J.P. Hill, H. Benthien, F.H.L. Essler, E. Jeckel-

- mann, H.S. Choi, T.W. Noh, N. Motoyama, K.M. Kojima, S. Uchida, D. Casa, and T. Cog, Phys. Rev. Lett. **92**, 137 402 (2004).
- ³⁶ H. Eskes, L.H. Tjeng, and G.A. Sawatzky, Phys. Rev. B **41**, 288 (1990).
- ³⁷ J. Ghijsen, L.H. Tjeng, J. van Elp, H. Eskes, J. Westerink, G.A. Sawatzky, and M.T. Czyzyk, Phys. Rev. B **38**, 11322 (1988).
- ³⁸ E.B. Stechel and D.R. Jennison, Phys. Rev. B **38**, 8873 (1988).
- ³⁹ A.K. McMahan, J.F. Annett, and R.M. Martin, Phys. Rev. B **42**, 6268 (1990).
- ⁴⁰ M.T. Czyzyk and G.A. Sawatzky, Phys. Rev. B **49**, 14211 (1994-II).
- ⁴¹ L.F. Mattheiss and D.R. Hamann, Phys. Rev. B **40**, 2217 (1989).
- ⁴² R. Hayn, H. Rosner, V. Yu. Yushankhai, S. Haffner, C. Duerr, M. Knupfer, G. Krabbes, M. S. Golden, J. Fink, H. Eschrig, D. J. Singh, N.T. Hien, A.A. Menovsky, Ch. Jung, and G. Reichardt, Phys. Rev. B **60**, 645 (1999).
- ⁴³ J.J.M. Pothuizen, R. Eder, N.T. Hien, M. Matoba, A.A. Menovsky, and G.A. Sawatzky, Phys. Rev. Lett. **78**, 717 (1997).
- ⁴⁴ C. Duerr, S. Legner, R. Hayn, S.V. Borisenko, Z. Hu, A. Theresiak, M. Knupfer, M. S. Golden, J. Fink, F. Ronning, Z.-X. Shen, H. Eisaki, S. Uchida, C. Janowitz, R. Mueller, R.L. Johnson, K. Rossnagel, L. Kipp, and G. Reichardt, Phys. Rev. B **63**, 014505-1 (2000).
- ⁴⁵ Albert W. Overhauser, Phys. Rev. **101**, 1702 (1956).
- ⁴⁶ M. Boman and R. J. Bursill, Phys. Rev. B **57**, 15167 (1998).
- ⁴⁷ V.I. Cherepanov, E.N. Kondrashov and A.S. Moskvina, Sov.Phys.-Solid State, **42**, 866 (2000).
- ⁴⁸ I.B. Bersuker and V.Z. Polinger, Vibronic Interactions in Molecules and Crystals, Springer-Verlag, Berlin, 1989.
- ⁴⁹ M.S. Hybertsen, M. Schluter, and N.E. Christensen, Phys. Rev. B **39**, 9028 (1989).
- ⁵⁰ M.S. Hybertsen, E.B. Stechel, M. Schluter, and D.R. Jennison, Phys. Rev. B **41**, 11068 (1990).
- ⁵¹ V.Yu. Yushankhai, V.S. Oudovenko, and R. Hayn, Phys. Rev. B **55**, 15562 (1997-I).
- ⁵² A.S. Davydov, Theory of Molecular Excitons, McGraw-Hill, New York, 1962.
- ⁵³ M. Martinez-Ripoli, S. Martinez-Carrera, and S. Garsia-Blanco, Acta Crystallogr. Sect. B **27**, 677 (1971).
- ⁵⁴ T. Boeske, O. Knauff, R. Neudert *et. al.*, Phys. Rev. B **56**, 3438 (1997).
- ⁵⁵ A. Fujimori, Y. Tokura, H. Eisaki, H. Takagi, S. Uchida, and M. Sato, Phys. Rev. Lett. **40**, (1989) 7303.
- ⁵⁶ S. Haffner, R. Neudert, M. Kielwein *et. al.*, Phys. Rev. B **57**, 3672 (1998).
- ⁵⁷ T. Boeske, K. Maiti, O. Knauff *et. al.*, Phys. Rev. B **57**, 138 (1997).
- ⁵⁸ S. LaRosa, I. Vobornik, F. Zwick *et.al.*, Phys. Rev. B **56**, R525 (1997).
- ⁵⁹ C. Kim, P.J. White, Z.-X. Shen *et. al.*, Phys. Rev. Lett. **80**, 4245 (1998).
- ⁶⁰ F. Ronning, C. Kim, D.L. Feng *et. al.*, Science **282**, 2067 (1998).
- ⁶¹ S. Haffner, D. M. Brammeier, C. G. Olson *et. al.*, Phys. Rev. B **61**, 14 378 (2000).
- ⁶² B.O. Wells, Z.-X. Shen, A. Matsuura, D. M. King, M. A. Kastner, M. Greven, and R. J. Birgeneau, Phys. Rev. Lett. **74**, 964 (1995).
- ⁶³ S. Atzkern, M. Knupfer, M.S. Golden *et. al.*, Phys. Rev. B **62**, 7845 (2000-II).
- ⁶⁴ Y. Mizuno, T. Tohyama, S. Maekawa *et. al.*, Phys. Rev. B **57**, 5326 (1998-I).
- ⁶⁵ R. Neudert, S.-L. Drechsler, J. Malek *et. al.*, Phys. Rev. B **62**, 10752 (2000-I).
- ⁶⁶ *Excitons*, E.I. Rashba, M.D. Sturge eds., NH, 1987.
- ⁶⁷ P.A. Fleury and R. Loudon, Phys. Rev. **166**, 514 (1968).
- ⁶⁸ R.V. Pisarev, I. Sanger, G. A. Petrakovskii, and M. Fiebig, Phys. Rev. Lett. **93**, 037204 (2004).
- ⁶⁹ M. Bassi, P. Camagni, R. Rolli, G. Samoggia, F. Parmigiani, G. Dhalenne, and A. Revcolevschi, Phys. Rev. B **54**, R11030 (1996-II).
- ⁷⁰ M. Knupfer, private communication.
- ⁷¹ R. Neudert, Ph.D. Thesis, University of Technology Dresden, 1999.
- ⁷² R. Neudert, M. Knupfer, M.S. Golden, J. Fink, W. Stephan, K. Penc, N. Motoyama, H. Eisaki, and S. Uchida, Phys. Rev. Lett. **81**, 657 (1998).
- ⁷³ A.K. McMahan, R.M. Martin, and S. Satpathy, Phys. Rev. B **38**, 6650 (1988).
- ⁷⁴ Jiro Tanaka, Koji Kamiya, and Chizuko Tanaka, Physica C **61**, 451 (1989).
- ⁷⁵ J. Tanaka and C. Tanaka, J. Phys. Chem. Solids **59**, 1861 (1998).
- ⁷⁶ J.P. Hill, C.-C. Kao, W.A.L. Caliebe, M. Matsubara, A. Kotani, J.L. Peng, and R.L. Greene, Phys. Rev. Lett. **80**, 4967 (1998).